

Enhancing Oxygen Reduction Reaction on Pt-Based Electrocatalysts through Surface Decoration for Improved OH Reduction Equilibrium and Reduced H₂O Adsorption

Yu-Jun Xu,¹ Chiao-An Hsieh,² Chen-Yu Zhang¹, Li-Dan Zhang,³ Han Tang,¹ Lu-Lu Zhang,¹ Jun Cai,¹ Yan-Xia Chen^{*,1}, Shuehlin Yau² and Zhi-Feng Liu^{*,3,4}

¹*Hefei National Research Center for Physical Sciences at Microscale, Department of Chemical Physics, University of Science and Technology of China, Hefei, 230026, China*

²*Department of Chemistry, National Central University, Jhongli 320, Taiwan*

³*Department of Chemistry and Centre for Scientific Modeling and Computation, Chinese University of Hong Kong, Shatin, Hong Kong, China*

⁴*Ganjiang Innovation Academy, Chinese Academy of Sciences, Ganzhou, Jiangxi, 341119, China*

Abstract: Electrochemical energy and substance conversion devices involve complex electrode processes, characterized by multiple charge transfer steps, competing pathways, and various intermediates. Such complexity makes it challenging to enhance electrocatalytic activity. The prevailing strategy typically focuses on optimizing the geometric and electronic structures of the electrocatalysts to align the adsorption energies of reaction intermediates with the peak of the activity Volcano curve. In this study, we demonstrate that surface decoration can effectively shape the micro reaction environment for the model system of oxygen reduction reaction (ORR) on Pt electrodes. By applying a partial hydrophobic I* adlayer on the Pt surface, we can shift the equilibrium of OH* reduction and weaken H₂O* adsorption, which significantly enhances ORR kinetics. With *in situ* scan tunneling microscopy (STM) and theoretical calculations, our study reveals the formation of isolated Pt₂ surface units situated in a hydrophobic valley surrounded by adsorbed iodine atoms. This minimalist Pt₂ active unit exhibits significantly greater activity for ORR compared to an extended Pt surface. This strategy could pave the way for developing highly efficient catalysts with potential applications in fuel cell technology and metal air batteries and extension to other electrochemical conversion reactions such as ammonia synthesis and CO₂ reduction.

*E-mail: yachen@ustc.edu.cn (Y.X.C.); zfliu@cuhk.edu.hk (Z.F.L.).

1. Introduction

Oxygen reduction reaction (ORR) is the primary cathodic reaction in many systems such as the fuel cells, metal air batteries, and electrochemical corrosion of metals. The catalysis of ORR has been a major challenge for decades, as the slow ORR rate imposes a kinetic bottleneck in the advancement of technologies such as fuel cells^{1, 2} and metal air batteries.^{3, 4} Significant efforts have been devoted to boost ORR kinetics through engineering the electrocatalyst materials and optimizing the ORR conditions.^{5, 6} The origins for its slow kinetics and the structure-activity relations of ORR catalysts have also been extensively investigated experimentally.⁷⁻⁹ Despite over a century of intensive research, the onset overpotential for ORR consistently exceeds 200 mV.^{10, 11}

Since 1980s, model studies examining the changes of ORR rates on crystalline metal surfaces have yielded a wealth of kinetic data related to well-characterized surface structures,^{10, 12} establishing ORR as a good test ground for validating various theoretical approaches aimed at elucidating electro-catalytic reactions from first principles. The widely used Computational Hydrogen Electrode (CHE) method, which calculates the reaction energy of proton-coupled electrode reactions, was first formulated for the ORR on Pt(111).¹³ Based on the thermochemical data obtained through CHE, linear scaling relationships between the binding energies for OOH*, O* and OH*, have been identified, linking the ORR activity to the adsorption energies of these oxygenated species. It produces a volcano curve that accounts for variations in ORR activity across different metals, with Pt, the best monometallic ORR catalyst, at the top of the curve.⁶ When applied to more complicated systems, such as bimetallic alloys,^{14, 15} Pt shells on metal core substrates,¹⁶⁻¹⁸ and various nano-structured catalysts,^{2, 19-22} these volcano curves have provided an effective strategy for enhancing ORR activities by tuning the metal bonding within the electrode, and consequently, the binding energy of oxygenated species. A well-known example is the Pt-skin structure, Pt₃Ni(111), which exhibits 10 times higher ORR activity than Pt(111) surface and a positive shift of half wave potential for ORR by ca. 100 mV, (Figure 1b),¹⁵ making it one of the most effective ORR catalysts to date.

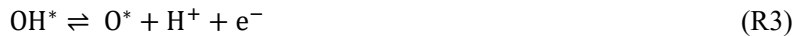
More recent calculations have gone beyond thermochemical values to probe the reaction mechanism. The results highlight the importance of H₂O, which is the main component at the ORR cathode/electrolyte interface. As the solvent of aqueous electrolyte and ion transport channels for solid polymer electrolyte membranes, as well as the product of ORR, the concentration of H₂O (ca. 55 M) is more than 4 orders of magnitude higher than that of O₂ (ca. 1 mM). In the kinetic region of ORR in acid solution, there is a fast acidic dissociation of adsorbed H₂O* on Pt(111) through



whose exchange current density is estimated to be around 50 mA cm⁻².^{10, 23} As demonstrated by Density Functional Theory (DFT) calculations, it opens up a hydrolysis reduction channel for O*^{24, 25}



which is in competition with the protonation of O*, the reverse reaction of the equilibrium



Recent ab initio molecular dynamics (AIMD) simulations reveal that at elevated electrode potentials, the reduction of O* is dominated by O* hydrolysis (R2) rather than O* protonation (R3).²⁶ Unfortunately, R2

does not generate electrochemical current, which is responsible for the irreversible oxide region in the cyclic voltammogram shown in Figure 1a. The current associated with $4e^-$ ORR can only be detected when the applied potential is negative to the E_{eq} for OH^* reduction (R1), rather than for O^* reduction, as illustrated in Figures 1b, 1c and 1d.¹⁰ These mechanistic insights suggest that H_2O^* is in fact detrimental to ORR, by diverting O^* reduction towards the hydrolysis channel, a conclusion supported by recent experiments at the Pt(111)/ionomer interface.²⁷ This also presents a significant challenge for the enhancement of ORR, as it is difficult to avoid the presence of H_2O in an aqueous environment, where it is both the solvent and the product.²⁸

In this work, we demonstrate an effective strategy to enhance ORR by shifting the equilibrium of R1 through the decoration of Pt electrode surfaces with I^* . Specifically, I^* is introduced onto the surface of Pt(hkl), pc-Pt and Pt nanoparticles as a submonolayer. Despite a significant portion of the surface Pt sites being covered by I^* , the overall ORR activity is effectively enhanced, with Pt(111)@0.31 ML I^* achieving the highest promotion factor, comparable to that of $Pt_3Ni(111)$, the best ORR alloy catalyst reported to date.¹⁵ These results challenge the prevalent view that strongly chemisorbed anions, such as I^* , diminish the ORR activity.^{29, 30} The dependence of the ORR promotion factor on the surface orientation of Pt(hkl) and coverage of I^* has been systematically investigated in both acidic and alkaline solutions. The mechanism is elucidated by *in situ* scan tunneling microscopy (STM), Fourier Transform infrared spectroscopy (FTIRS) and DFT calculations, indicating the prospect for simultaneously enhancing ORR and reducing Pt contents.

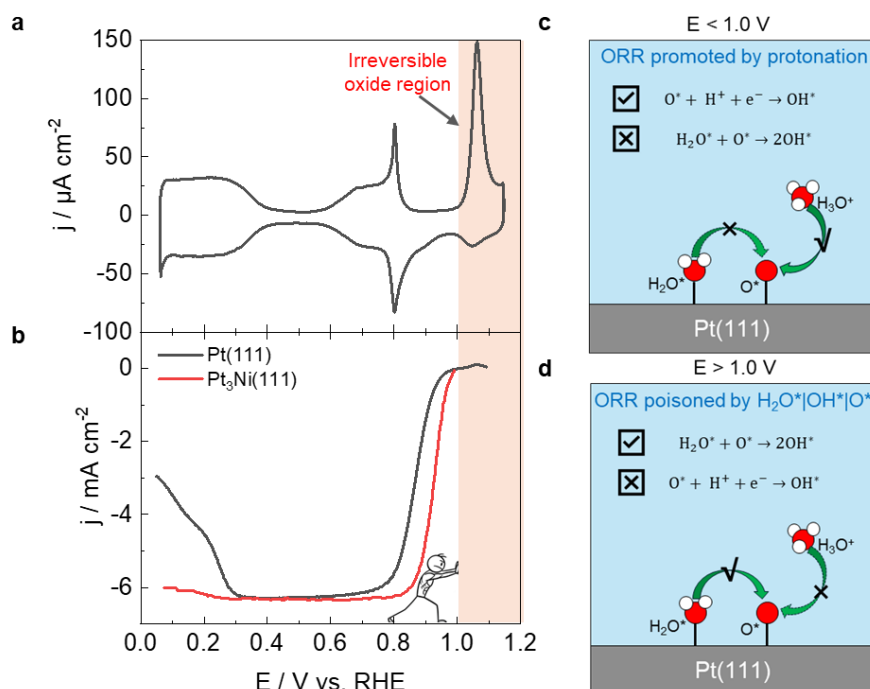


Figure 1. Oxygen reduction reaction mechanism diagram. (a) Cyclic voltammogram, (b) representative ORR polarization curves for Pt(111) and $Pt_3Ni(111)$ electrode in 0.1 M $HClO_4$, schematic illustration of the mechanisms for the dominating (c) O^* protonation channel at $E < 0.8$ V and (d) O^* hydrolysis channel at $E > 0.8$ V. j - E curve for ORR at Pt_3Ni is adapted from Ref¹⁵ with permission from the publisher.

2. Results and Discussion

2.1 Electrochemical characterization of Pt(111)@ I^* electrodes

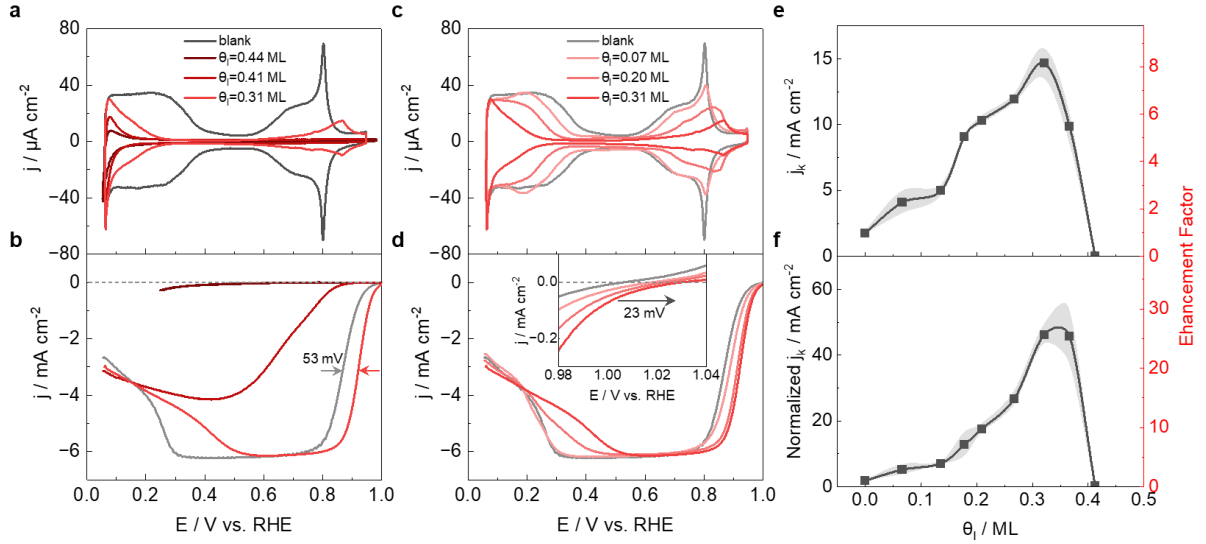


Figure 2. Cyclic voltammograms and oxygen reduction reaction activities of Pt@ x ML I*. (a, c) CVs of Pt(111) electrodes modified by I* with various coverages. (b, d) Polarization curves for ORR recorded in the positive scan in O₂ saturated 0.1 M HClO₄. Inset: detailed view of kinetic region of ORR polarization curves and the shift of the onset potential for ORR. The scan rate is 50 mV/s. For the ORR experiments, the electrode rotation rate is 1600 rpm. (e, f) The j_k of Pt@ x ML I* electrode normalized to the (e) geometric area and (f) free active sites as well as the corresponding enhancement factor in reference to that at Pt(111) at 0.9 V. Free active sites are estimated based on the H_{UPD} charge. The shadows indicate error bars in (e) and (f) represent the standard deviation of three independent measurements.

Shown in Figure 2 are the CVs for Pt(111) partially covered by I* and the corresponding polarization curve at various surface coverages. The iodide adsorption on the Pt electrode surface can be considered as an oxidation process,



This is supported by DFT calculations that iodine atom is the actual adsorbate on Pt(111), with a small electron transfer (0.08 to 0.13 e/atom) to the surface (see also evidences given in Figure S1 and below).^{31, 32} As shown in Figures 2a and 2b, there is almost no ORR activity when Pt(111) surface is fully covered with iodine ($\theta_I = 0.44$ ML, see also Figure S2), as is well known in the literature.^{30, 32} When θ_I is reduced to 0.41 ML, the partially covered Pt(111) first shows activity towards $2e^-$ ORR, producing H₂O₂. Further reduction in θ_I to 0.31 ML shows enhanced activity towards $4e^-$ ORR process, producing higher current than that on a clean Pt(111) electrode (Figures 2b and 2d). The Pt(111)@I* system thus goes full spectrum, from ORR passivation, to $2e^-$ ORR, to $4e^-$ ORR, with decreasing iodine coverage. This clearly demonstrate that whether I* is a poisoning or a promoter depends on the coverage.

The more interesting change happens in the $4e^-$ ORR region, shown in Figures 2b and 2d. The polarization curve shifts to the rightmost, soon after ORR switches from $2e^-$ to $4e^-$ process around $\theta_I = 0.31$ ML. Afterwards, the j - E curves for ORR moves gradually to the left with decreasing coverage, towards the curve obtained on a clean Pt(111). All these curves reach a diffusion-limiting plateau for $E = 0.3\sim 0.8$ V, with the ORR diffusion limiting current (j_L) exactly the same as that on clean Pt(111), while both the onset potential (inset in Figure 2d) and the half-wave potential for ORR (Figure 2d) shift positively with increasing θ_I , up to ca. 0.31 ML. Such a trend is quite counterintuitive: the more surface sites of Pt(111) electrode are covered with I*, the better is its ORR activity.

Nonetheless, the corresponding CVs, as shown in Figures 2a and 2c, are roughly similar to that of clean Pt(111). The region with the electrode potential $E = 0.05\sim 0.4$ V is due to the under-potential deposition of hydrogen (H_{UPD}). The region of $E = 0.6\sim 1.0$ V is due to hydroxyl (OH^*) formation through R1. Separating these two is a double layer charging region with $E = 0.4\sim 0.6$ V. Compared to the CV of clean Pt(111), the onset of H_{UPD} region is pushed to lower E with increasing I^* coverage. The decrease in the integral charge density for H_{UPD} in the potential region from 0.4 V to 0.05 V provides a way to estimate θ_I , as is well confirmed that the coverage of H_{UPD} amounts to 2/3 ML at 0.05 V.³³ The calculated values, as shown in Figures 2a and 2c, are in line with those estimated from STM results discussed below. In the OH^* region, the current peak for OH^* formation is pushed toward higher potentials as θ_I increases, and the higher I^* surface coverage is also indicated by the decrease in the integral charge density for OH^* formation.

The ORR kinetic current (j_k) free of mass transfer effect can be estimated based on the Kouteckey-Levich Equation:³⁴

$$j_k = (j_L - j) / (j_L \cdot j) \quad (1)$$

where j is the measured current density for ORR at a given potential. The Tafel slope can be obtained from the plot of $\log(j_k)$ vs the electrode potential (see Figure S3). For θ_I from 0 up to 0.37 ML, the value of Tafel slope is around 50 mV/dec, in agreement with previously reported value for $4e^-$ ORR on unmodified Pt(111).³⁵ More exactly, the Tafel slope gradually decreases from 55 mV/dec at $\theta_I = 0$ to 46 mV/dec at $\theta_I = 0.31$ ML, as the ORR activity is promoted by partial I^* coverage. The ratio of j_k for ORR at 0.9 V versus that on clean Pt(111), is usually taken as the promoting factor for the comparison of ORR activity.¹⁵ As plotted in Figure 2e, the factor is far below 1 at $\theta_I = 0.41$ ML, when the ORR going through a $2e^-$ process. It then jumps up at $\theta_I = 0.37$ ML and soon reaches a maximum at $\theta_I = 0.31$ ML, with a promotion factor of 8.8, close to the promotion factor ~ 10 reported on Pt_3Ni (111) where the first layer of surface atoms are all composed of Pt (Figure 2e).¹⁵ Furthermore, when normalizing the kinetic ORR current to the available active sites calculated by the reduction in H_{UPD} coverage, the promotion factor for Pt(111)@0.31 ML I^* reaches 28.6 (Figure 2f). Thus the normalized ORR activity on Pt(111) partially covered by iodine outperforms that on Pt_3Ni (111), the best Pt based ORR catalyst reported so far.¹⁵ When the measurement is conducted in 0.1 M $HClO_4$ solution with 0.1 mM KI, similar to the conditions reported before,^{30, 32, 36} we are able to reproduce the results of ORR suppression and I^- oxidation to I_2 and IO_x^- above 0.8 V, as Pt(111) is completely covered by I^* due to continuous exposure to I^- (Figure S2).

Present findings are in strong contrast with previous reports where it was found that anions in the solution phase, such as halides, sulfate, nitrate, and (bi)phosphate, are often chemisorbed on electrode surfaces, which reduce ORR activities.^{12, 37, 38} The general opinion in the literature is that fine tuning the metallic bonds by mixing electropositive elements usually promotes catalysis, while covalent bonding, such as the adsorption of electronegative species, is often deleterious.^{30, 39, 40} There are, however, a few intriguing exceptions. Markovic and coworkers demonstrated that the chemisorption of CN^- on Pt(111) enhanced the ORR activity by blocking the adsorption of spectator anions.⁴¹ More surprising were the reports showing the promotion of ORR activity by the moderate coverage of sulfide on Pt/C and Pt black electrodes,^{42, 43} even though sulfur is one of the worst poisons for many catalysts. Similar promotion effects were also observed

more recently with moderate coverage of Br and Cl on Pt(111).⁴⁴ However, the promotion factors in these cases are modest, compared to that achieved on Pt₃Ni alloy. The ORR enhancement by CN⁻ surface patterning on Pt(111) was observed in H₂SO₄ and H₃PO₄ solutions, while for the more active ORR in HClO₄ solution, there was little improvement over Pt(111).⁴¹ More significantly, there is limited understanding of the underlying mechanisms, even though these results challenge our current conception of catalytic poisons. Without such understandings, it's difficult to formulate strategies for ORR enhancement by surface decorations.

2.2 Scan tunneling microscopy measurement of Pt(111)@I*

Iodine is also a well-known catalytic poison that passivates Pt at full coverage (Figure 2b), but fortunately, the relevant surface structures have been models for chemisorption and extensively investigated by STM and other surface science techniques.⁴⁵⁻⁴⁸ To unravel why I* with submonolayer coverage enhances ORR activity, we have carried out *in situ* STM studies to examine the microscopic structure of the iodine adlayer on the Pt(111) electrode in electrochemical environment.

Two samples are prepared and examined separately, for comparison. Sample #1 produces an iodine adlayer with a surface coverage of $\theta_I \approx 0.36$ ML, according to the charge flow in the H_{UPD} process. The surface state of this sample potentiostated at 0.4 V is revealed by STM images shown in Figure 3a. Three patches of ordered arrays (I, II, and III) and scattered disarrays are noted. The symmetry of the structure seen in domain I is defined by the rhombic cell, characterized as $(\sqrt{7} \times \sqrt{7})R19.1^\circ$ with $\theta_I = 0.43$ ML. That of domain II has the same symmetry, but is rotated by 38° . The hexagonal array seen in domain III is characterized as $(\sqrt{3} \times \sqrt{3})R30^\circ$ with $\theta_I = 0.33$ ML. The ball model of the $(\sqrt{7} \times \sqrt{7})R19^\circ$, $(\sqrt{3} \times \sqrt{3})R30^\circ$ are shown in Figures 3f and 3g. Similar adsorbate domain structures has also been confirmed for images taken at 0.7 V or even higher potentials (Figure S5). These two types of iodine structures have been reported before.⁴⁵⁻⁴⁷

If these two structures are equally populated, the coverage would be 0.38 ML, slightly higher than 0.36 ML determined by the charge of H_{UPD}. The discrepancy is due to the uncounted packing defects in the iodine arrays, imaged as depressions in the STM images. Furthermore, a series of STM images acquired at 0.7 V (Figure S5) reveal that this iodine adlayer was unstable against protracted STM scanning. The ordered iodine arrays could be interconverted and defects migrated on the Pt electrode. Such movements could be too fast to be tracked by the STM, which caused fuzziness in STM imaging.

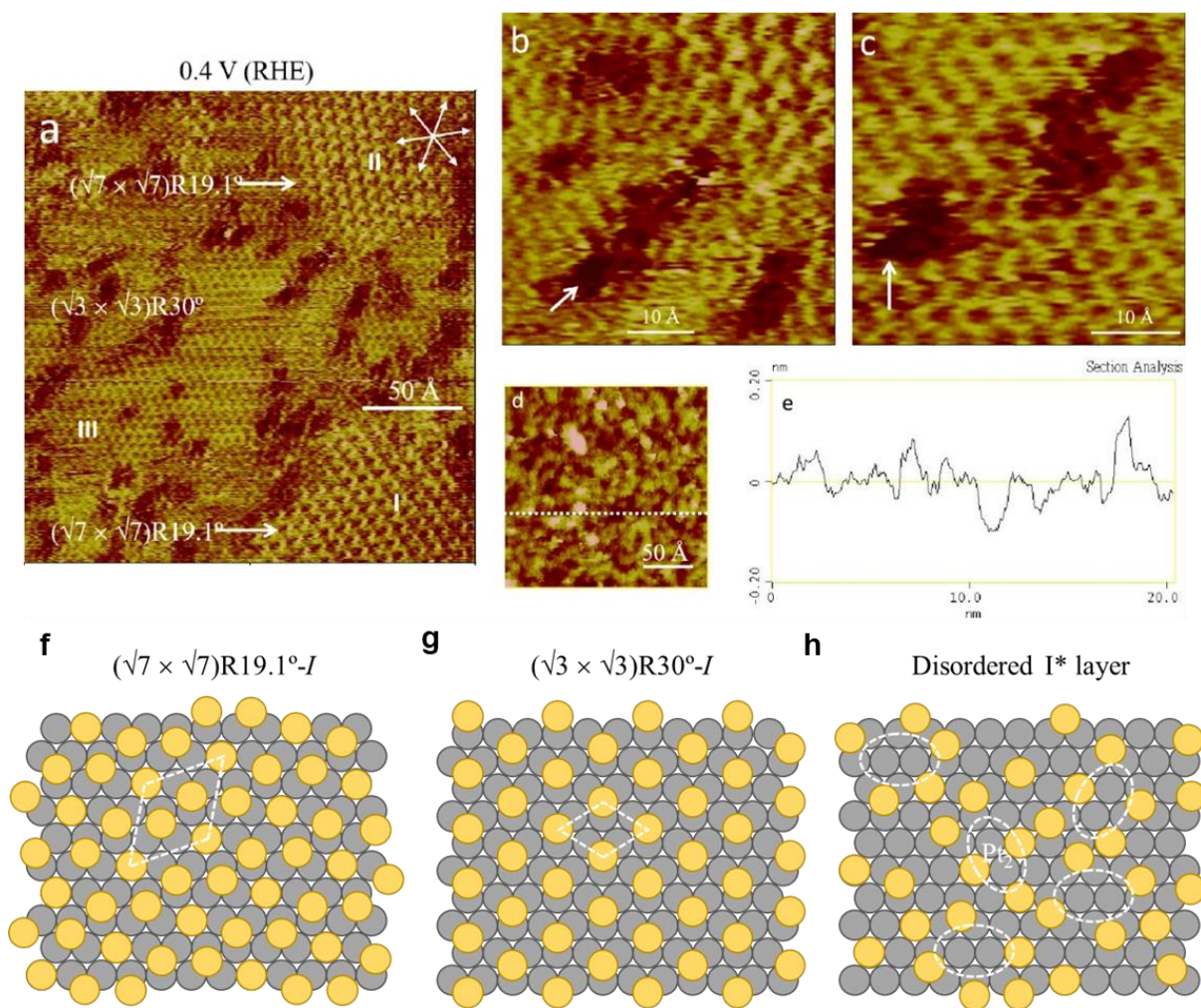


Figure 3. In situ STM images of Pt@ x ML I*. In situ STM images showing the structures of iodine adlayer on two Pt(111) samples with high (a-c) and low (d, e) iodine coverages. The former is mostly covered with ordered $(\sqrt{3} \times \sqrt{3})R30^\circ$ and $(\sqrt{7} \times \sqrt{7})R19.1^\circ$ - I structures, while the latter is disordered. Depressions seen with sample #1 are highlighted in (b) and (c). Panel (d) reveals the general morphology of sample #2. Panel (e) shows the corrugation profile along the dotted line marked in (d). The potential of Pt is 0.4 V and STM imaging with -200 mV bias voltage and 1 nA feedback current. Panel (f-h) is a ball model of the $(\sqrt{7} \times \sqrt{7})R19.1^\circ$, $(\sqrt{3} \times \sqrt{3})R30^\circ$ - I and disordered I* layer structure with Pt atoms and I adatoms are colored in grey and yellow, respectively.

Defects in the iodine adlayer on sample #1 are mostly seen at the domain boundaries between the $(\sqrt{7} \times \sqrt{7})R19.1^\circ$ and $(\sqrt{3} \times \sqrt{3})R30^\circ$ or inside the $(\sqrt{3} \times \sqrt{3})R30^\circ$ domains. They are further examined by high-resolution STM scans (Figures 3b and 3c). Only a handful of pits (indicated by arrows) in a 60×60 Å scan area are ~ 1.1 Å lower than the neighboring $(\sqrt{3} \times \sqrt{3})R30^\circ$ array. These are vacancies in the iodine adlayer, which are accessible to oxygen molecules, and subsequently play a vital role in catalyzing ORR. Close examination of Figures 3b and 3c reveals that weak spots ~ 0.6 Å lower than iodine adatom are present inside these depressions, which could be iodine adatoms in disarrays or ORR intermediates such as O^* or OH^* .

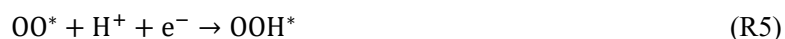
In situ STM scan at 0.4 V in 0.1 M $HClO_4$ solution (open to the air) reveals a completely disordered iodine adlayer, as shown in Figure 3d. Neither switching to a different scan area nor sweeping the potential between 0.1 and 1 V affect the structure of the iodine adlayer. The iodine adlayer has corrugated, rolling-hill morphology with I* aggregating into clusters with poorly defined shapes and dimensions (Figure S6).

Obviously, sample #2 has more vacancy defects in the iodine adlayer than sample #1, which is probably linked to its higher ORR activity, as described above (Figure 2). The cross-section profile shown in Figure 3e reveals the surface roughness of sample #2. Most depressions are ~ 1.2 Å lower than I* and ~ 6 Å wide, suggesting that no more than 3 Pt atoms are exposed, since the average Pt–Pt bond distance is ca. 2.8 Å.⁴⁹ ⁵⁰ The possible ball model of $\theta_I = 0.33$ ML is shown in Figure 3h. The surface roughness of sample #2 becomes more evident, as the corrugation height increases from 1.2 to 2.5 Å upon dosing with O₂ (Figure S7). This result is thought to result from the reaction between iodine adatoms and oxygen molecules, producing uncharacterized oxide species on the Pt electrode.

2.3 Promotion mechanism of Pt(111)@I* electrode

As a model system, ORR on Pt(111) has been explored recently by AIMD simulations, with explicit water molecules and real-time treatment of the dynamic effects.^{24, 26, 51} These mechanistic understandings are very relevant to the ORR on the Pt(111)@I* system. The key step separating 2e[−] and 4e[−] paths is the breaking of the O–O bond. On Pt(111), such a dissociation is facile when O₂* is on a side-on configuration (as in Figure S8b), leading to the production of two separate O* atoms and their eventual reduction to H₂O along the 4e[−] path.²⁶ It also means that for 4e[−] ORR, a Pt₂ surface unit is required to stabilize these two O* atoms.

The complete passivation of ORR on Pt(111)@I* with $\theta_I > 0.44$ ML is obviously due to the blocking of all the Pt sites by iodine atoms, as well documented in the literature.^{30, 32} The initial reduction of θ_I from 0.44 ML produces isolated single Pt sites separated from each other, which can now take up O₂ in an end-on configuration, rather than the side-on configuration which requires a Pt₂ unit. On such a single Pt site, only one O end is bonded to the surface, as shown in Figure S8a, and the dissociation of O₂ is prohibited, since a single Pt site cannot accommodate two O* atoms. When it picks up a proton to form OOH*,



2e[−] ORR is initiated. A further step of proton attack would reduce OOH* to H₂O₂, and produce the typical 2e[−] polarization curve, with the current at the diffusion limit being about half of that for the 4e[−] curve (compare curves in Figure 2b at $\theta_I = 0.41$ ML and at blank). When θ_I is reduced below 0.41 ML, 4e[−] ORR soon becomes the dominant process (at $\theta_I = 0.37$ ML, Figure S4). The catalytic activity peaks around $\theta_I = 0.31$ ML. This trend can be attributed to the increasing population of Pt₂ sites on Pt(111)@I*, as observed in STM experiments (Figures 3b–3d). With more side-on O₂* adsorption structures formed (Figure S8b), the path to O–O dissociation and 4e[−] ORR is now open.

The I* layer on Pt consists of iodine atoms, and their adsorption on the surface is chemisorption. Tkatchenko *et al* demonstrated by DFT calculations that the iodine-surface bond is covalent, with a chemisorption energy of ~ 2.6 eV (60 kcal/mol).³¹ Interestingly, there is a small charge transfer (< 0.1 e) from iodine to the Pt surface, despite the higher electronegativity of I (2.66) compared to Pt (2.28). This can be explained by the fact that I* is bonded to multiple Pt atom in typical fcc or hcp adsorption configurations, as verified by our own calculations (see Figure S9). Chemisorption I* blocks the active sites on the surface, which is responsible for the catalytic poisoning effect observed at full coverage. However, the covalent bonding transfers a small amount of charge to the surface (Table S1). The d-band center for uncovered

surface Pt atom decreases upon I* adsorption by 0.2 eV at $\theta_I = 0.31$ ML (see Table S2). This change in electronic structure is similar to placing Pt skin on Ni crystals, which decreases the d-band center by 0.1~0.3 eV, depending on the surface index.¹⁵ Thus, while iodine atoms cover some Pt sites by covalent bonding, they do not negatively impact the catalytic activity of the uncovered Pt sites. This is likely also true for the chemisorption of S* or Br*, as their electronegativities (2.58 for S and 2.96 for Br) are close to that of I. It is overly simplistic to claim that covalent bonding on Pt surface inherently poison its catalytic activity.

On the contrary, in the case of Pt(111)@I* systems, iodine-Pt(111) covalent bonding significantly enhances the ORR activity of the uncovered Pt sites nearby. Between $\theta_I = 0 \sim 0.31$ ML, the ORR activity increases significantly as θ_I is raised (Figure 2e). This observation is counter-intuitive, as increasing coverage reduces Pt sites available for O₂ adsorption and its subsequent reduction. The number of available Pt sites for ORR should be the largest at $\theta_I = 0$ ML. Yet, the ORR activity of a clean Pt(111) is only 1/9 of that at $\theta_I = 0.31$ ML (Figure 2e) (The intrinsic enhancement of ORR activity after normalization to the number of free active sites is ca. 28.8 times, Figure 2f). Obviously, the presence of I* on Pt(111) promotes ORR, when it's a submonolayer (with $\theta_I < 0.41$ ML).

There are two aspects for this enhancement effect. The first is the steepening of the ORR polarization curve, as mentioned earlier, with the Tafel slope decreasing from 55 mV/dec at $\theta_I = 0$ ML to 46 mV/dec at $\theta_I = 0.31$ ML. The second aspect is a small shift of the onset potential, by about 23 mV at maximum, as shown in the inset of Figure 2d. Both are related to the overall ORR mechanism, as recently elucidated by AIMD studies, in which the adsorbed H₂O* plays a significant role, as mentioned in the introduction. The environment for the adsorption of H₂O is significantly different on clean Pt(111) from that on I@Pt systems.

On clean Pt(111), there are plenty Pt sites for O₂*, O* and H₂O*. With H₂O being the solvent, it is impossible to avoid H₂O* and its poisonous effect through O* hydrolysis. However, a Pt₂ site on Pt(111)@I* is surrounded by I* atoms which are almost neutral and do not interact much with H₂O molecules. After the formation of O* atoms by the dissociation O–O* bond, the O* hydrolysis is blocked by the absence of H₂O* nearby. It enhances the branching ratio of the O* protonation channel (the reverse of R3) and produces more ORR current. Between $\theta_I = 0 \sim 0.31$ ML, the increase in I* coverage reduces the presence of H₂O* and its poisonous effect, which increases the contribution of O* protonation and thus the ORR current, as indicated by the decreases in the Tafel slope, from 55 mV/dec at $\theta_I = 0$ ML, to 46 mV/dec at $\theta_I = 0.31$ ML. In this coverage region, the reduction of H₂O* poisonous effect is more important for ORR current than the increase of Pt active sites.

The shift in the onset potential is related to R1, the equilibrium between the acidic dissociation of H₂O* and the OH* reduction to H₂O*. The reverse reaction is required for the completion of ORR. We have calculated the reaction free energy for R1 on clean Pt(111) and on Pt(111)@I* with $\theta_I = 0.25$ ML, by CHE method,¹³ employing an adsorbate solvated by three H₂O molecules, as shown in Figure S10. In terms of the structure, the main difference between Pt(111) and Pt(111)@I* is that two of the H₂O molecules are adsorbed on clean Pt(111), while none of the H₂O molecules are adsorbed on Pt(111)@I*. The calculated ΔG for OH* reduction is -0.55 eV on clean Pt(111), and -0.86 eV on Pt(111)@I*. When the model is expanded to four H₂O molecules, as shown in Figure S11, the free energy is -0.62 eV on clean Pt(111) and -0.68 eV on Pt(111)@I*. In both cases, OH* reduction is more favorable on Pt(111)@I*.

The desorption of H_2O^* is also needed to clear Pt sites for O_2 adsorption, although this step itself does not generate current. In this regard, H_2O can again be considered as a catalytic poison, and the weaker its adsorption energy, the better the ORR activity. On a clean Pt(111), H_2O^* adsorption is energetically favorable by 0.53 eV, in agreement with values previously reported.⁵² This value decreases with increasing number of I^* on the surface: 0.52 eV for one I ($1/16 = 0.06$ ML), 0.45 eV for three I ($3/16 = 0.19$ ML), 0.25 eV for four I ($1/4 = 0.25$ ML), and 0.11 eV for five I ($5/16 = 0.31$ ML). Therefore, both the reduction of OH^* to H_2O^* and the desorption of H_2O^* are facilitated by the weakened H_2O^* adsorption on Pt(111) partially covered by I^* , which is responsible for the upward shift in the onset potential for ORR, as shown in Figure 2d.

2.4 The hydrophobicity of $\text{Pt}@\text{I}^*$

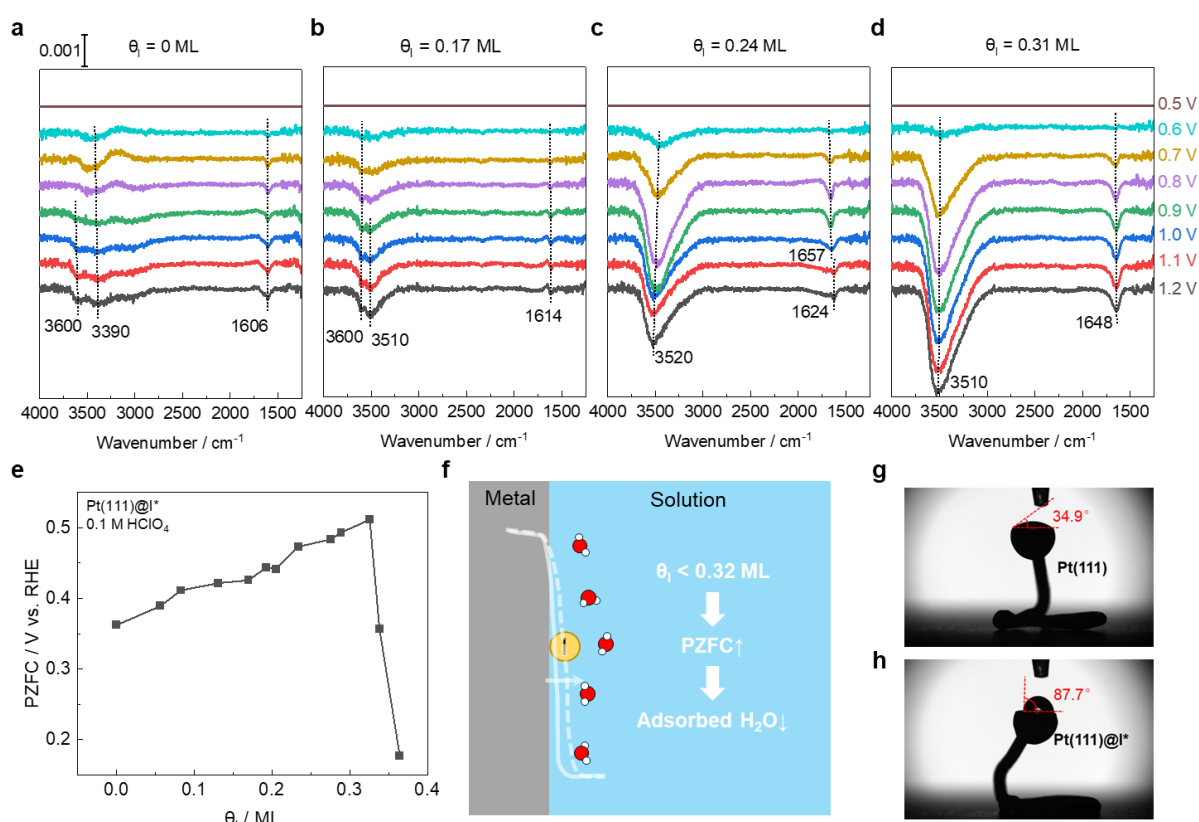


Figure 4. Evidence for the hydrophobicity of adsorbed I^* atoms. (a-d) In situ ATR-SEIRAS spectra were recorded for the Pt working electrode in an Ar-saturated solution at potentials from 1.2 to 0.5 V (vs. RHE) at different I^* coverages. The IR background was taken at 0.5 V in the corresponding solution. (e) PZFC of the $\text{Pt(111)}@x \text{ ML } \text{I}^*$ electrode as a function of I^* coverage. (f) Schematic illustration of the reduced adsorption of water molecules and the change in electron spillover from the electrode at low I^* coverage. (g, h) Results of contact angle measurements for Pt(111) and $\text{Pt}@\text{I}^*$.

In order to verify whether I^* mitigates water adsorption at Pt electrode, we have also examined the $\text{Pt}@\text{I}^*$ interface using electrochemical in-situ surface-enhanced infrared absorption spectroscopy (SEIRAS) in the attenuated total reflection (ATR) configuration. Shown in Figures 4a-4d are the spectra at various coverages with $\theta_{\text{I}} = 0, 0.17, 0.24$ and 0.31 ML respectively, which were estimated from CV (Figure S12). In each case, the spectrum at 0.5 V, shown as a straight line, is taken as the background and subtracted from the original spectrum which contains much contribution from the solvent H_2O molecules. The signals from

adsorbed H_2O^* are better revealed in such difference spectra. On polycrystalline Pt thin film electrode (Figure 4a) without I^* exposure, small negative peaks are observed around 1606 cm^{-1} for the bending mode and around 3390 cm^{-1} for the O–H stretching mode. The small decrease in these signals at higher electrode potential is due to the acidic dissociation of H_2O^* , by R1, to produce OH^* , a process well documented in its CV.⁵³ On Pt electrode with $\theta_{\text{I}} = 0.31\text{ ML}$ (Figure 4d), these peaks are significantly more negative, indicating the absence of H_2O^* on iodine covered Pt surface. Comparing Figure 4b at $\theta_{\text{I}} = 0.17\text{ ML}$, Figure 4c at $\theta_{\text{I}} = 0.24\text{ ML}$, and Figure 4d at $\theta_{\text{I}} = 0.31\text{ ML}$, the decrease is more pronounced at higher coverage, consistent with the expectation of less H_2O^* at increased iodine coverage.

The decrease in H_2O^* adsorption is also indicated by the shift in the potential of zero free charge (PZFC). Experimentally, it has been established that H_2O^* adsorption lowers the PZFC for Pt(111), as the electrostatic repulsion between the electrons from oxygen atoms in water and those on Pt(111) impedes the electron spillover across Pt(111)/water interface, and consequently lowers its surface potential (work function).^{54, 55} We have measured the PZFC of clean Pt(111) and Pt(111)@ I^* with varying θ_{I} in HClO_4 solution, using $\text{S}_2\text{O}_8^{2-}$ (Peroxydisulfate, PDS) reduction as the probe reaction (Figure S13), a well-documented procedure for Pt electrodes.⁵⁶ A higher and a lower PZFC for the Pt(111)/0.1 M HClO_4 interface are identified, and the lower PZFC shift positively with increasing θ_{I} up to ca. 0.32 ML (Figure 4e).⁵⁷ On clean Pt(111), the lower PZFC is 0.37 V, in agreement with previous reports.⁵⁶ Between $\theta_{\text{I}} = 0.0\text{ ML}$, i.e. clean Pt(111), and Pt(111)@ I^* with $\theta_{\text{I}} = 0.32\text{ ML}$, the PZFC is shifted upward by ca. 150 mV. Considering that adsorbed iodine atoms only transfer a small amount of charge to Pt (0.08 to 0.13 e/atoms),³¹ and one adsorbed I^* displace several adsorbed water, this increase is likely due to a reduction in H_2O^* adsorption with increasing θ_{I} (Figure 4f). Notably, PZFC decreases only when θ_{I} exceeds 0.32 ML, as water adsorption reaches a minimum at high I^* coverage, making the electronic effect of I^* on Pt the dominating factor.⁵⁷

In fact, the hydrophobic nature of Pt(111)@ I^* can be observed in a simple experiment: the measurement of contact angle. As illustrated in Figures 4g and 4h the contact angle for a water drop is larger on iodine covered Pt(111) than that on a clean Pt(111) surface.

It should be noted that Hoshi and co-workers have systematically investigated the effect of introducing organic hydrophobic groups to Pt crystal electrodes, based on the idea that these groups can affect the water structure near the electrode surface and thus the ORR activity.⁵⁸ The promotion factor is moderate for various organic compounds, such as amines,⁵⁹ alkanes,⁶⁰ and aromatic molecules.⁶¹ However, one tetraalkylammonium cation, THA^+ (tetra-*n*-hexylammonium), stands out with an impressive promotion factor of 8.⁶² We were intrigued by this result, since in the same report, it showed that N(alkyl)_4^+ cations with shorter alkyl chains, such as methyl, ethyl, or *n*-butyl groups, only produced moderate enhancement. While trying to verify these results, we found that the THA^+ used in the report was contaminated by iodide and the promotion effect was actually due to I^* , rather than THA^+ (See SI for reviewer only). Nonetheless, these organic hydrophobic groups can have moderate enhancement for ORR, likely by a mechanism similar to that discussed above, although with their bulky structures, it's challenging to control the surface coverage and the availability of isolated Pt_2 sites for the maximization of promotion effect.

2.5 Beyond Pt(111) single crystal electrode and acid media

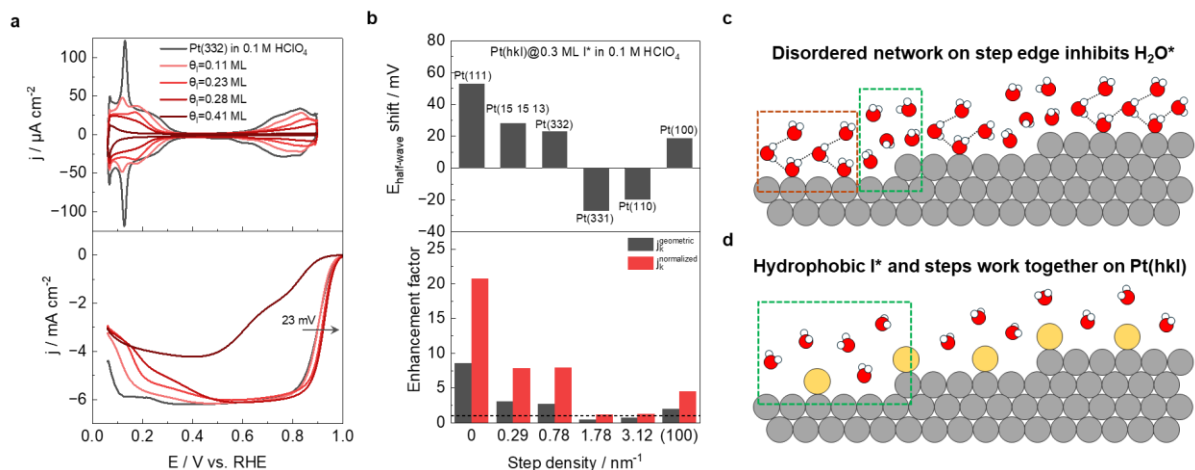


Figure 5. Activity trends and mechanisms of Pt(hkl)@ x ML I* electrodes. (a) CVs and ORR polarization curves recorded in the positive scan in 0.1 M HClO₄ of Pt(hkl)@ x ML I* electrodes. The scan rate is 50 mV/s. For the ORR experiments, the electrode rotation rate is 1600 rpm. (b) The shift of half-wave potential and the enhancement factor of j_k at 0.9 V plotted against the step density of Pt(hkl)@ 0.3 ML I* electrodes. (c) Schematic illustration of water molecule adsorption on high-index single crystal electrode surfaces with/without I*-modification.

The ORR enhancement by I* submonolayer is also observed on Pt(hkl) surfaces in acid solution. For (111) stepped single crystal electrodes, the ORR activity correlates with the step density, as shown in Figure 5a and 5b. At an I* coverage of 0.30 ML, surfaces with low step density, such as Pt(332) and Pt(15 15 13), exhibit significant enhancement and positive shift in half-wave potential. In contrast, on surfaces with high step intensity, such as Pt(311) and Pt(110), ORR is either less enhanced or even suppressed (see Figure 5b). The presence of (111) terrace is not always required, as enhancement is also observed on Pt(100)@0.30 ML I*, although the promotion factor is smaller than that on Pt(111) (Figure S14). However, no enhancement is observed on polycrystalline Pt electrodes (Figure S15).

For clean Pt(hkl), it has been reported that the ORR activity of clean Pt(hkl) surfaces increases with higher step density, reaching a maximum on Pt(331).⁶³ This enhancement is attributed to the disruption of the ordered H₂O* network by the step edge, which destabilizes H₂O* and facilitates the removal of OH* (Figure 5c). However, such a trend is reversed on I* covered Pt(hkl) surfaces, since the presence of I* weakens H₂O* adsorption on (111) terraces, as illustrated in Figure 5d, which can promote ORR. I* could also adsorb near the step edge, making its effects on H₂O* and ORR an interesting topic for future research.

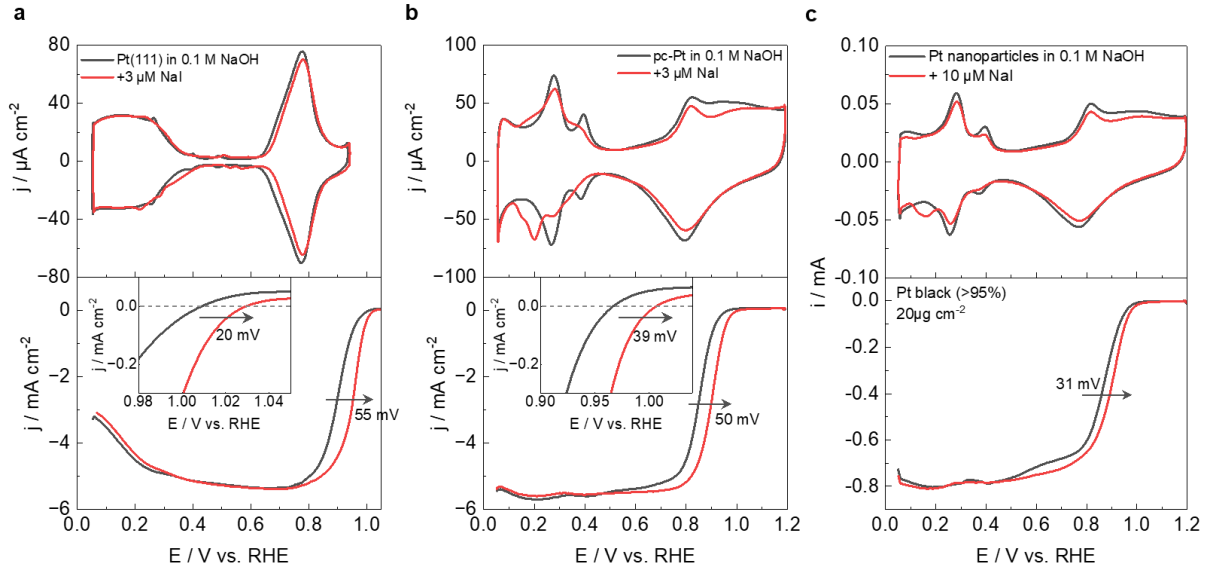


Figure 6. Activity of Pt electrode in 0.1 M NaOH with/without NaI. (a) CVs and ORR polarization curves recorded in the positive scan for (a) Pt(111) electrode in 0.1 M NaOH with/without 3 μM NaI, (b) polycrystalline Pt electrode in 0.1 M NaOH with/without 3 μM NaI and (c) Pt nanoparticles electrode in 0.1 M NaOH with/without 10 μM NaI. Inset: detailed view of kinetic region of ORR polarization curves and the shift of the onset potential for ORR. The scan rate is 50 mV/s. For the ORR experiments, the electrode rotation rate is 1600 rpm.

In alkaline solution, similar enhancement of ORR activity is not only observed on I^{*}-modified Pt(111), but also on electrodes composed of polycrystals and nanoparticles Pt, as shown in Figure 6. The half-wave potential for ORR shows a positive shift upon the addition of NaI, by 55, 50, and 31 mV, and the promotion factor is ca.4.0, 6.2 and 2.2 for j_k at 0.9 V, respectively. The ORR mechanism on Pt(111) in alkaline media has also been studied by AIMD recently, showing a 4e⁻ pathway similar to that in the acid solution.⁵¹ The symmetric peaks at 0.78 V_{RHE} in Fig.6a can be attributed to the OH^{*} adsorption/desorption,



corresponding to (R1) in the acid case. O^{*} reduction can also produce current by



corresponding to (R3) in the acid case. However, above the equilibrium potential of (R6), OH⁻ would be adsorbed on Pt(111) via the reverse of (R6). R7 followed by the adsorption of OH⁻ leads also to an overall reaction of O^{*} hydrolysis (R2), with no net electrochemical current produced. The onset potential for ORR is again determined by OH^{*} reduction (i.e. desorption), rather than by O^{*} reduction, and the presence of H₂O^{*} is also deleterious for ORR in alkaline media. Furthermore, OH^{*} desorption is not achieved by the breaking of Pt–OH^{*} bond. Rather it is facilitated by the formation of Pt–OH₂^{*}, which leaves a solvated OH⁻ in the outer sphere through proton migration.⁵¹ The desorption of H₂O^{*} is again the final step of ORR. Therefore, it's not surprising that the hydrophobic I^{*} improves the ORR performance by suppressing R2 and promoting R7 in alkaline solution, shifting up the ORR onset potential by 20 and 39 mV on Pt(111) and polycrystalline Pt (inset in Figures 6a and 6b).

While in acid solution the enhancement effect of I^{*} is favored on (111) terrace, in alkaline solution, it is observed on all morphological forms. This lack of facet selectivity may be attributed to the preferential

adsorption of hydroxyl anions on edge sites, which leaves I* on the flat terraces and weakens H₂O* adsorption in those areas as well.⁶⁴ These results demonstrate that surface decoration can be an effective ORR enhancement strategy on Pt(hkl), polycrystal-Pt and nanoparticle Pt electrodes, especially in alkaline solution.

3. Conclusions

We have shown that Pt electrodes partially covered by iodine can enhance ORR activity, with a promotion factor close to the performance of the best alloy ORR electrode, Pt₃Ni(111). With I* coverage systematically varied, the link between the decrease in H₂O* adsorption and the increase in ORR activity is established by experimental measurements on Pt(111), especially by in-situ STM and in-situ vibrational spectra and supported by DFT calculations. These results demonstrate one possible answer to the challenge of H₂O* poisoning on electrode surface during ORR, predicted by recent mechanistic studies. By embedding active Pt₂ sites in the valley of I@Pt and protecting these sites from solvent H₂O molecules, it is possible to achieve a more than eight-fold increase in ORR activity, despite the ~70% reduction of active Pt sites.

Such a catalyst model for ORR runs counter to two commonly held assumptions. First, it is often assumed that the formation of covalent bonds between non-metal atoms with Pt surface is deleterious for its catalytic activity. I* is indeed a well-known catalytic poison for ORR on Pt, as the chemisorption of iodine atom on Pt can easily take up all the Pt sites. However, our study shows that the bonding interaction between I* and Pt surface in itself does not poison the nearby Pt sites. In fact, it promotes ORR, because Pt has a relatively large electronegativity among metals and I* actually donates a small amount of charge to Pt surface. Furthermore, the presence of I* on partially cover Pt(111) lessens H₂O* adsorption on uncovered Pt sites and enhances ORR by reducing the poisonous effect of H₂O*. This is likely also the mechanism for the ORR enhancement previously observed on Pt electrodes partially covered by S* and Br*, indicating the potential of using even non-metal atoms either in surface decoration or as substrate to tune the OH* reduction energy and the H₂O* adsorption energy.

Second, it is also often assumed that increasing surface area would enhance catalytic activity. But in the case of ORR, extended Pt surface makes it hard to avoid H₂O* adsorption. Four electron ORR needs Pt₂ as its basic catalytic unit, so that both O* atoms in O₂* or OOH* interact with Pt atoms and O–O bond breaking is facilitated. Nearby Pt sites would attract H₂O* adsorption, which reduces ORR current. Instead of extended Pt surface, an improved strategy is to create an ensemble of active Pt₂ units, isolated from each other and situated on non-Pt substrate surrounded by hydrophobic adsorbates, as shown in Figure S8d. Such a catalyst can enhance the ORR activity by mitigating water poisoning, while lowering the platinum content to a minimum, both being much desirable goals in the advancement of fuel cell technology.

Acknowledgments

This work was supported by the National Natural Science Foundation of China (no. 22372154, 22172151), by the Research Grants Council of Hong Kong SAR Government (GRF Grant 14303114), by the Ministry of Science and Technology of the People's Republic of China (G2022200006L), and by the National Science

and Technology Council of ROC (NSTC 112-2113-M-008-005). We are grateful for the generous allocation of computer time on the HPC clusters at the Center for Scientific Modeling and Computation, CUHK.

References:

- (1) Kodama, K.; Nagai, T.; Kuwaki, A.; et al. Challenges in Applying Highly Active Pt-Based Nanostructured Catalysts for Oxygen Reduction Reactions to Fuel Cell Vehicles. *Nat. Nanotechnol.* **2021**, *16*, 140.
- (2) Wang, X. X.; Swihart, M. T.; Wu, G. Achievements, Challenges and Perspectives on Cathode Catalysts in Proton Exchange Membrane Fuel Cells for Transportation. *Nat. Catal.* **2019**, *2*, 578.
- (3) Wang, Q.; Kaushik, S.; Xiao, X.; Xu, Q. Sustainable Zinc–Air Battery Chemistry: Advances, Challenges and Prospects. *Chem. Soc. Rev.* **2023**, *52*, 6139.
- (4) Kongara, A.; Samuel, A. K.; Kapadia, G.; Chandiran, A. K. Mechanically Rechargeable Zinc-Air Batteries for Two- and Three-Wheeler Electric Vehicles in Emerging Markets. *Commun. Mater.* **2024**, *5*, 244.
- (5) Shao, M.; Chang, Q.; Dodelet, J.-P.; Chenitz, R. Recent Advances in Electrocatalysts for Oxygen Reduction Reaction. *Chem. Rev.* **2016**, *116*, 3594.
- (6) Kulkarni, A.; Siahrostami, S.; Patel, A.; Nørskov, J. K. Understanding Catalytic Activity Trends in the Oxygen Reduction Reaction. *Chem. Rev.* **2018**, *118*, 2302.
- (7) Briega-Martos, V.; Herrero, E.; Feliu, J. M. Effect of Ph and Water Structure on the Oxygen Reduction Reaction on Platinum Electrodes. *Electrochim. Acta* **2017**, *241*, 497.
- (8) Gómez-Marín, A. M.; Rizo, R.; Feliu, J. M. Oxygen Reduction Reaction at Pt Single Crystals: A Critical Overview. *Catal. Sci. Technol.* **2014**, *4*, 1685.
- (9) Schmidt, T. J.; Stamenkovic, V.; Arenz, M.; et al. Oxygen Electrocatalysis in Alkaline Electrolyte: Pt(Hkl), Au(Hkl) and the Effect of Pd-Modification. *Electrochim. Acta* **2002**, *47*, 3765.
- (10) Chen, W.; Huang, J.; Wei, J.; et al. Origins of High Onset Overpotential of Oxygen Reduction Reaction at Pt-Based Electrocatalysts: A Mini Review. *Electrochem. Commun.* **2018**, *96*, 71.
- (11) Wu, G.; Zelenay, P. Activity Versus Stability of Atomically Dispersed Transition-Metal Electrocatalysts. *Nat. Rev. Mater.* **2024**, *9*, 643.
- (12) Marković, N.; Ross Jr, P. Surface Science Studies of Model Fuel Cell Electrocatalysts. *Surf. Sci. Rep.* **2002**, *45*, 117.
- (13) Nørskov, J. K.; Rossmeisl, J.; Logadottir, A.; et al. Origin of the Overpotential for Oxygen Reduction at a Fuel-Cell Cathode. *J. Phys. Chem. B* **2004**, *108*, 17886.
- (14) Huang, X.; Zhao, Z.; Cao, L.; et al. High-Performance Transition Metal–Doped Pt₃Ni Octahedra for Oxygen Reduction Reaction. *Science* **2015**, *348*, 1230.
- (15) Stamenkovic, V. R.; Fowler, B.; Mun, B. S.; et al. Improved Oxygen Reduction Activity on Pt₃Ni (111) Via Increased Surface Site Availability. *Science* **2007**, *315*, 493.
- (16) Wang, J. X.; Inada, H.; Wu, L.; et al. Oxygen Reduction on Well-Defined Core–Shell Nanocatalysts: Particle Size, Facet, and Pt Shell Thickness Effects. *J. Am. Chem. Soc.* **2009**, *131*, 17298.
- (17) Stephens, I. E.; Bondarenko, A. S.; Perez-Alonso, F. J.; et al. Tuning the Activity of Pt (111) for Oxygen Electroreduction by Subsurface Alloying. *J. Am. Chem. Soc.* **2011**, *133*, 5485.
- (18) Wang, H.; An, W. Promoting the Oxygen Reduction Reaction with Gold at Step/Edge Sites of Ni@Aupt Core–Shell Nanoparticles. *Catal. Sci. Technol.* **2017**, *7*, 596.
- (19) Li, M.; Zhao, Z.; Cheng, T.; et al. Ultrafine Jagged Platinum Nanowires Enable Ultrahigh Mass Activity for the Oxygen Reduction Reaction. *Science* **2016**, *354*, 1414.
- (20) Chen, C.; Kang, Y.; Huo, Z.; et al. Highly Crystalline Multimetallic Nanoframes with Three-Dimensional Electrocatalytic Surfaces. *Science* **2014**, *343*, 1339.
- (21) Tang, M.; Zhang, S.; Chen, S. Pt Utilization in Proton Exchange Membrane Fuel Cells: Structure Impacting Factors and Mechanistic Insights. *Chem. Soc. Rev.* **2022**, *51*, 1529.
- (22) Liu, G.; Shih, A. J.; Deng, H.; et al. Site-Specific Reactivity of Stepped Pt Surfaces Driven by Stress Release. *Nature* **2024**, *626*, 1005.
- (23) Yang, F.; Liao, L.-w.; Li, M.-f.; et al. Kinetics Study on O₂ Adsorption and Ohad Desorption at Pt (111), Its Implication to Oxygen Reduction Reaction Kinetics. *Chin. J. Chem. Phys.* **2014**, *27*, 479.
- (24) Cheng, T.; Goddard, W. A.; An, Q.; et al. Mechanism and Kinetics of the Electrocatalytic Reaction Responsible for the High Cost of Hydrogen Fuel Cells. *Phys. Chem. Chem. Phys.* **2017**, *19*, 2666.

- (25) Sha, Y.; Yu, T. H.; Merinov, B. V.; et al. Oxygen Hydration Mechanism for the Oxygen Reduction Reaction at Pt and Pd Fuel Cell Catalysts. *J. Phys. Chem. Lett.* **2011**, *2*, 572.
- (26) Li, Y.; Liu, Z.-F. Solvated Proton and the Origin of the High Onset Overpotential in the Oxygen Reduction Reaction on Pt (111). *Phys. Chem. Chem. Phys.* **2020**, *22*, 22226.
- (27) Xu, Y.; Zhang, L.; Chen, W.; et al. Boosting Oxygen Reduction at Pt (111)| Proton Exchange Ionomer Interfaces through Tuning the Microenvironment Water Activity. *ACS Appl. Mater. Interfaces* **2024**, *16*, 4540.
- (28) Wang, H.; Li, H.; Duan, J.; et al. Adjustment of Molecular Sorption Equilibrium on Catalyst Surface for Boosting Catalysis. *Acc. Chem. Res.* **2025**, *58*, 440.
- (29) Marković, N.; Gasteiger, H.; Grgur, B.; Ross, P. Oxygen Reduction Reaction on Pt (111): Effects of Bromide. *J. Electroanal. Chem.* **1999**, *467*, 157.
- (30) Cui, H.; Chen, Y.-X. Deciphering the Linear Relationship in the Activity of the Oxygen Reduction Reaction on Pt Electrodes: A Decisive Role of Adsorbates. *J. Energy Chem.* **2024**, *94*, 70.
- (31) Tkatchenko, A.; Batina, N.; Cedillo, A.; Galván, M. Charge Transfer and Adsorption Energies in the Iodine–Pt (1 1 1) Interaction. *Surf. Sci.* **2005**, *581*, 58.
- (32) Sun, C.; Wen, R.; Qin, Y.; et al. Origin of Pt Site Poisoning by Impurities for Oxygen Reduction Reaction Catalysis: Tailored Intrinsic Activity of Pt Sites. *ACS Appl. Energy Mater.* **2023**, *6*, 5700.
- (33) Climent, V.; Feliu, J. M. Thirty Years of Platinum Single Crystal Electrochemistry. *J. Solid State Electrochem.* **2011**, *15*, 1297.
- (34) Chen, W.; Cui, H.-W.; Liao, L.-W.; et al. Challenges in Unravelling the Intrinsic Kinetics of Gas Reactions at Rotating Disk Electrodes by Koutecky–Levich Equation. *J. Phys. Chem. C* **2023**, *127*, 16235.
- (35) Wang, J. X.; Markovic, N. M.; Adzic, R. R. Kinetic Analysis of Oxygen Reduction on Pt(111) in Acid Solutions: Intrinsic Kinetic Parameters and Anion Adsorption Effects. *J. Phys. Chem. B* **2004**, *108*, 4127.
- (36) Inukai, J.; Osawa, Y.; Wakisaka, M.; et al. Underpotential Deposition of Copper on Iodine-Modified Pt (111): In Situ Stm and Ex Situ Leed Studies. *J. Phys. Chem. B* **1998**, *102*, 3498.
- (37) Zorko, M.; Farinazzo Bergamo Dias Martins, P.; Connell, J. G.; et al. Improved Rate for the Oxygen Reduction Reaction in a Sulfuric Acid Electrolyte Using a Pt (111) Surface Modified with Melamine. *ACS Appl. Mater. Interfaces* **2021**, *13*, 3369.
- (38) Kamat, G. A.; Zamora Zeledón, J. A.; Gunasooriya, G. K. K.; et al. Acid Anion Electrolyte Effects on Platinum for Oxygen and Hydrogen Electrocatalysis. *Commun. Chem.* **2022**, *5*, 20.
- (39) Tong, Y. J. Unconventional Promoters of Catalytic Activity in Electrocatalysis. *Chem. Soc. Rev.* **2012**, *41*, 8195.
- (40) Zangwill, A. *Physics at Surfaces*; Cambridge University Press, 1988.
- (41) Strmcnik, D.; Escudero-Escribano, M.; Kodama, K.; et al. Enhanced Electrocatalysis of the Oxygen Reduction Reaction Based on Patterning of Platinum Surfaces with Cyanide. *Nat. Chem.* **2010**, *2*, 880.
- (42) Park, I. S.; Tong, Y. Y. J. Sulfide-Adsorption-Enhanced Oxygen Reduction Reaction on Carbon-Supported Pt Electrocatalyst. *Electrocatalysis* **2013**, *4*, 117.
- (43) Wang, Y.-Y.; Chen, D.-J.; Tong, Y. J. Mechanistic Insight into Sulfide-Enhanced Oxygen Reduction Reaction Activity and Stability of Commercial Pt Black: An in Situ Raman Spectroscopic Study. *ACS Catal.* **2016**, *6*, 5000.
- (44) Cui, H.; Chen, Y.-X. Fighting Poison with Poison: Enhancing the Performance of Oxygen Reduction Reaction on Pt(111) Via Trace Halide Ion Addition. *J. Power Sources* **2025**, *625*, 235719.
- (45) Schardt, B. C.; Yau, S.-L.; Rinaldi, F. Atomic Resolution Imaging of Adsorbates on Metal Surfaces in Air: Iodine Adsorption on Pt (111). *Science* **1989**, *243*, 1050.
- (46) YAU, S.-L.; Vitus, C.; Schardt, B. In Situ Scanning Tunneling Microscopy of Adsorbates on Electrode Surfaces: Images of the ($\sqrt{3} \times \sqrt{3}$) R30°-Iodine Adlattice on Platinum (111). *J. Am. Chem. Soc.* **1990**, *112*, 3677.
- (47) Lu, F.; Salaita, G. N.; Baltruschat, H.; Hubbard, A. T. Adlattice Structure and Hydrophobicity of Pt (111) in Aqueous Potassium Iodide Solutions: Influence of Ph and Electrode Potential. *J. Electroanal. Chem. Interfacial. Electrochem.* **1987**, *222*, 305.
- (48) Magnussen, O. M. Ordered Anion Adlayers on Metal Electrode Surfaces. *Chem. Rev.* **2002**, *102*, 679.

- (49) Papoian, G.; Nørskov, J. K.; Hoffmann, R. A Comparative Theoretical Study of the Hydrogen, Methyl, and Ethyl Chemisorption on the Pt(111) Surface. *J. Am. Chem. Soc.* **2000**, *122*, 4129.
- (50) Brizuela, G.; Hoffmann, R. C5H5 on a Pt (111) Surface: Electronic Structure and Bonding. *J. Phys. Chem. A* **1998**, *102*, 9618.
- (51) Li, Y.; Liu, Z.-F. Cross-Sphere Electrode Reaction: The Case of Hydroxyl Desorption During the Oxygen Reduction Reaction on Pt(111) in Alkaline Media. *J. Phys. Chem. Lett.* **2021**, *12*, 6448.
- (52) Lew, W.; Crowe, M. C.; Karp, E.; Campbell, C. T. Energy of Molecularly Adsorbed Water on Clean Pt (111) and Pt (111) with Coadsorbed Oxygen by Calorimetry. *J. Phys. Chem. C* **2011**, *115*, 9164.
- (53) Osawa, M.; Tsushima, M.; Mogami, H.; et al. Structure of Water at the Electrified Platinum–Water Interface: A Study by Surface-Enhanced Infrared Absorption Spectroscopy. *J. Phys. Chem. C* **2008**, *112*, 4248.
- (54) Li, P.; Huang, J.; Hu, Y.; Chen, S. Establishment of the Potential of Zero Charge of Metals in Aqueous Solutions: Different Faces of Water Revealed by Ab Initio Molecular Dynamics Simulations. *J. Phys. Chem. C* **2021**, *125*, 3972.
- (55) Petrii, O. Zero Charge Potentials of Platinum Metals and Electron Work Functions. *Russ. J. Electrochem* **2013**, *49*, 401.
- (56) Martínez-Hincapié, R.; Climent, V.; Feliu, J. M. Peroxodisulfate Reduction as a Probe to Interfacial Charge. *Electrochem. Commun.* **2018**, *88*, 43.
- (57) Xu, Y.-J.; Zhang, S.; Zhang, M.-K.; et al. P-Block Elements Adsorption Induced Shift of Potential of Zero Free Charge of Pt(111)/HClO₄ Interface. *Electrochim. Acta* **2025**, *537*, 146858.
- (58) Hoshi, N.; Nakamura, M. Enhancement of the Activity for the Oxygen Reduction Reaction on Well-Defined Single Crystal Electrodes of Pt by Hydrophobic Species. *Chem. Lett.* **2021**, *50*, 72.
- (59) Wada, N.; Nakamura, M.; Hoshi, N. Structural Effects on the Oxygen Reduction Reaction on Pt Single-Crystal Electrodes Modified with Melamine. *Electrocatalysis* **2020**, *11*, 275.
- (60) Wada, N.; Kumeda, T.; Nakamura, M.; Hoshi, N. Effects of the Alkane on the Oxygen Reduction Reaction on Well-Defined Pt Surfaces. *Electrochemistry* **2020**, *88*, 265.
- (61) Takeda, T.; Nakamura, M.; Hoshi, N. The Oxygen Reduction Reaction on Pt Single Crystal Electrodes Modified with Aromatic Organic Molecules. *Electrochemistry* **2018**, *86*, 214.
- (62) Kumeda, T.; Tajiri, H.; Sakata, O.; et al. Effect of Hydrophobic Cations on the Oxygen Reduction Reaction on Single-Crystal Platinum Electrodes. *Nat. Commun.* **2018**, *9*, 4378.
- (63) Bandarenka, A. S.; Hansen, H. A.; Rossmeisl, J.; Stephens, I. E. Elucidating the Activity of Stepped Pt Single Crystals for Oxygen Reduction. *Phys. Chem. Chem. Phys.* **2014**, *16*, 13625.
- (64) Sarabia, F. J.; Sebastián, P.; Climent, V.; Feliu, J. M. New Insights into the Pt (Hkl)-Alkaline Solution Interphases from the Laser Induced Temperature Jump Method. *J. Electroanal. Chem.* **2020**, *872*, 114068.

Supporting Materials for
Enhancing Oxygen Reduction Reaction on Pt-Based Electrocatalysts
through Surface Decoration for
Improved OH Reduction Equilibrium and Reduced H₂O Adsorption

Yu-Jun Xu,¹ Chiao-An Hsieh,² Chen-Yu Zhang¹, Li-Dan Zhang,³ Han Tang,¹ Lu-Lu Zhang,¹ Jun Cai,¹ Yan-Xia
Chen*,¹, Shuehlin Yau² and Zhi-Feng Liu*,^{3,4}

¹*Hefei National Research Center for Physical Sciences at Microscale, Department of Chemical Physics,
University of Science and Technology of China, Hefei, 230026, China*

²*Department of Chemistry, National Central University, Zhongli 320, Taiwan*

³*Department of Chemistry and Centre for Scientific Modeling and Computation, Chinese University of Hong
Kong, Shatin, Hong Kong, China*

⁴*Ganjiang Innovation Academy, Chinese Academy of Sciences,
Ganzhou, Jiangxi, 341119, China*

*E-mail: yachen@ustc.edu.cn (Y.X.C.); zfliu@cuhk.edu.hk (Z.F.L.).

Supporting results

1. Facts that support I* adatoms at Pt(111)@x ML I* are almost electroneutral

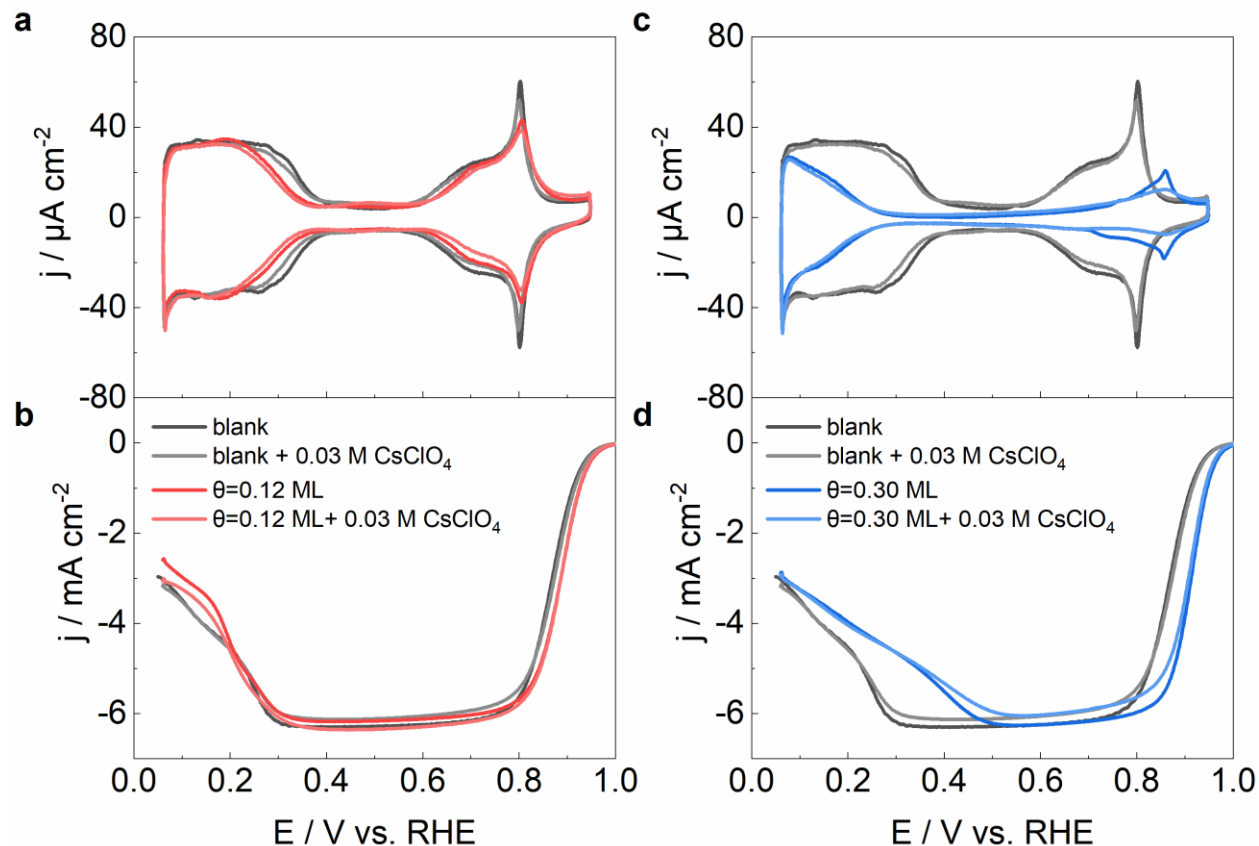


Figure S1. (a, c) CVs and (b, d) positive-going j -E curves for ORR at Pt(111)@x ML I*/0.1 M HClO₄ interfaces with and without addition of 0.03 M CsClO₄. For comparison, the base CV and the j -E curve for ORR at bare Pt(111) are also included in (a, c) and (b, d). The scan rate is 50 mV/s. For the ORR experiments, the rotation rate is 1600 rpm.

The base CVs of Pt@ x ML I* as well as the j -E curves for ORR with and without addition of CsClO₄ is nearly the same, this further supports that I* is nearly neutral, electrostatic interaction among I* and Cs⁺ is negligibly small. DFT calculation on the charge transfer for I* at the fcc site of Pt, determined from the Hirshfeld partitioning method, also suggests that the iodine atom remains almost neutral upon adsorption.^{1, 2, 3} This is in good agreement with previous report that I* at Pt(111) are largely neutral atoms, as evident by the negligible amount of ions is found in the thin liquid film after the electrode is immersed out from the electrolyte.⁴ This is also supported by the fact that when Cs⁺ is added into the electrolyte, ORR activity does not show obvious change (Figure S1).

It is well confirmed by the fact that there is significant current flow through the external circuit when such electrode is pulled out from the electrolyte with 0.1 mM KI.⁴ The current comes from the discharging of the charges initially stored in the electrochemical double layer (EDL) when the EDL breaks due to the pulling action. In contrast, for other species with anions as their adsorbing state, due to strong electrostatic interactions, liquid film with the whole EDL will be dragged out upon immersion out the solutions, under such circumstances, since there is no breakage of EDL no charge flows through the external circuit.

2. The poisoning effect of halogen on ORR kinetics of Pt(111) electrode

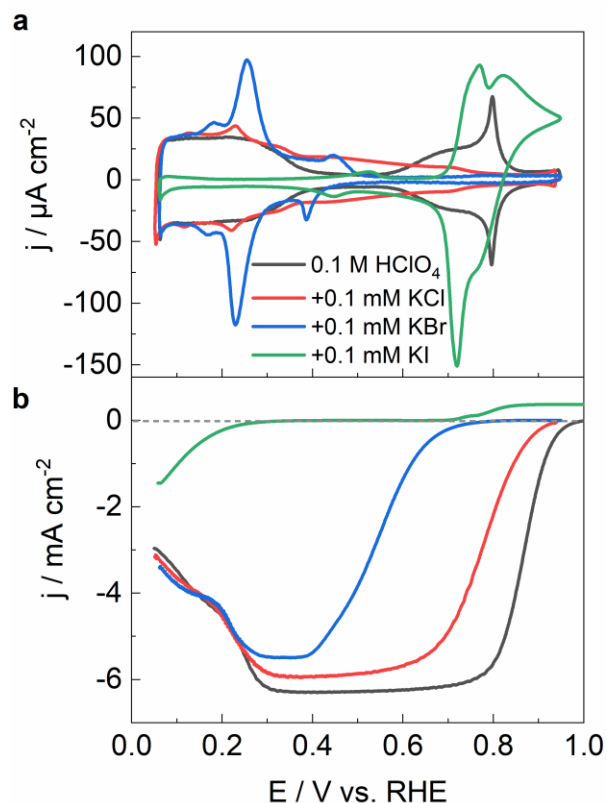


Figure S2. (a) CVs of Pt(111) electrodes and (b) positive-going j - E curves for ORR in 0.1 M HClO₄ + 0.1 mM KX (X= Cl, Br, I),. For comparison, the base CV and the j - E curve for ORR at bare Pt(111) are also included in (a) and (b). The scan rate is 50 mV/s. For the ORR experiments, the rotation rate is 1600 rpm.

Figure S2 shows the CVs and ORR polarization curves in 0.1 M HClO₄ with addition of 0.1mM KX (X=Cl, Br, I) respectively. The j - E curve shifts significantly to the negative potentials even though only 0.1 mM KX is added into the solution. With addition of KX with the same concentration, the extent for the inhibition of ORR at Pt(111) decreases in the order of KI > KBr > KCl, this is in good agreement with previous reports.^{3, 5, 6}

In solution with 0.1 M HClO₄ + 0.1 mM KI, Pt(111) surface is fully saturated with I* in the potential regime from 0.3 V to 1.0 V. In O₂ free solution, the anodic current at $E > 0.7$ V is from the oxidation of I⁻ to I₂, subsequently I₂ combines I⁻ to form I₃⁻ ($3\text{I}^- \leftrightarrow \text{I}_3^- + 2\text{e}^-$). The cathodic current in the same potential regime is due to reduction of I₃⁻ to I⁻ ($\text{I}_3^- + 2\text{e}^- \leftrightarrow 3\text{I}^-$), as in good agreement with previous reports.⁷.

The pair of small redox peak at ca. 0.5 V is also quite similar to previous observation, is probably related to the phase transition of I* adlayer.⁸ In O₂ containing solutions the redox between I₃⁻ and I⁻ are superimposed with ORR, since ORR current is tenth of times higher, its contribution is masked.

Since in solution with 0.1 M HClO_4 + 0.1 mM KI, Pt(111) surface is fully saturated with I^* in the potential regime from 0.3 V to 1.0 V, no ORR current is observed at $E > 0.3$ V when this solution is saturated with O_2 . At $E < 0.3$ V, cathodic current due to partial reduction of O_2 to H_2O_2 can be observed. This is probably due to desorption of some I^* , which leads to free active sites for O_2 adsorption and reduction.

In contrast for the case with 0.1 M HClO_4 + 0.1 M KBr, desorption of Br^* is seen at potentials below 0.5 V. For the case with 0.1 M HClO_4 + 0.1 M KCl, desorption of Cl^* is seen at potentials below 0.8 V. Accordingly, comparing to the case with Pt(111)@saturated I^* adlayer, ORR current at the same potential is less poisoned by Cl^* and Br^* .

3. The variation in the Tafel slope of ORR at Pt(111)@I* with changes in I* coverage

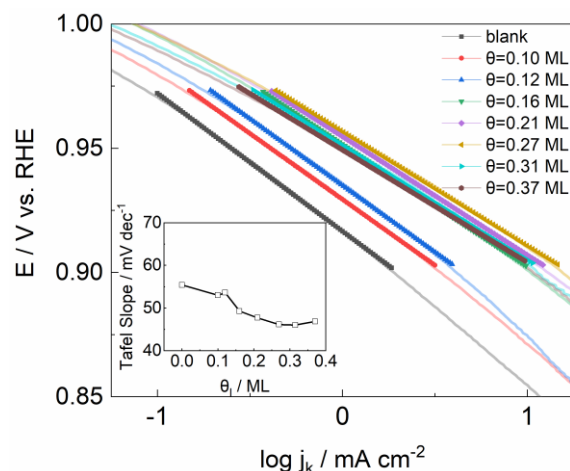


Figure S3. Tafel plots of polarization curves for ORR at Pt(111)@x ML I* / 0.1 M HClO₄ interfaces recorded in the positive scan. The point lines are fits of the curves from which the indicated Tafel slopes are obtained. Inset: the relationship between ORR Tafel slopes and I* coverages.

The Tafel slope for ORR has a value around 55 mV/dec at blank Pt(111) (Figure S3) in acidic media, in agreement with previously reported value for ORR on clean Pt(111). The Tafel slope decreases with increasing I* coverage, reaching 46 mV/dec at 0.31 ML. The change in Tafel slope indicates that the ORR kinetics increase with rising coverage, suggesting a stronger preference for the protonation channel over the hydration channel as coverage increases.

5. EC-STM reveals I* adlayer at Pt(111) has defined domain structures as well as defects between domain boundaries, the latter probably acts at ORR active sites

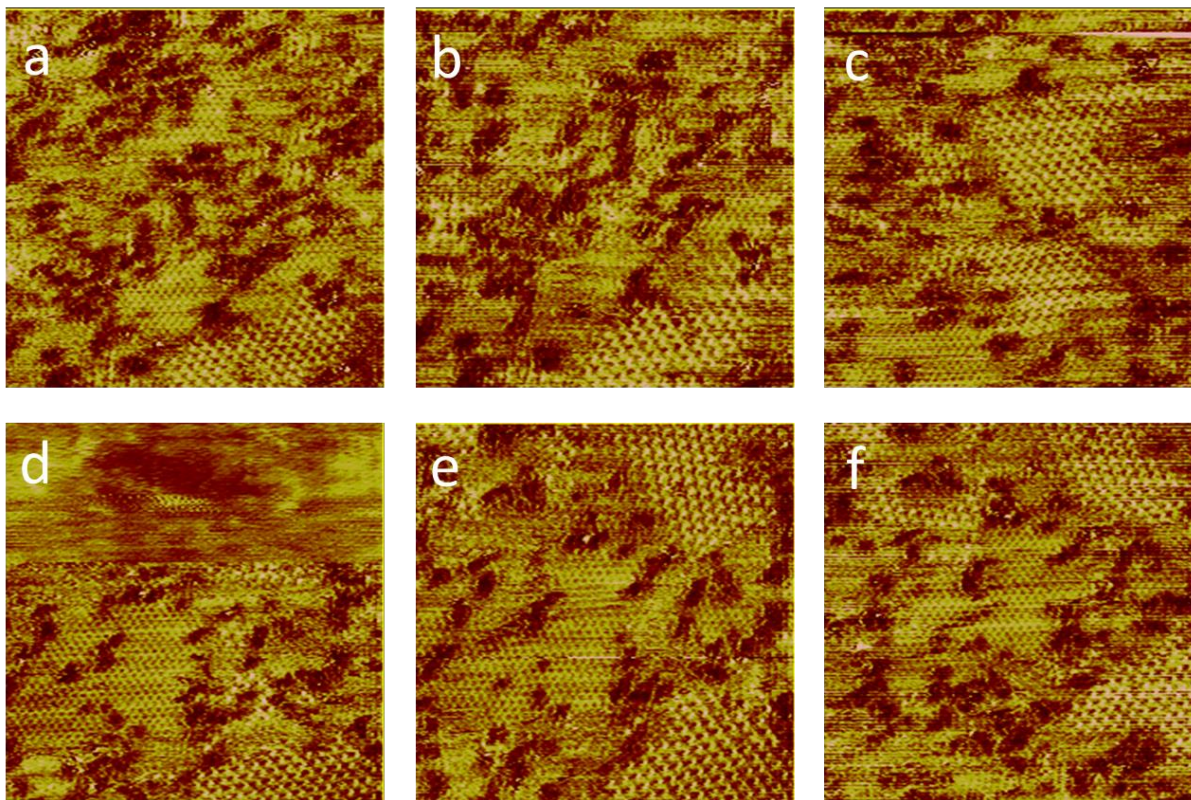


Figure S5. A series of STM images showing the constant restructuring of the iodine adlayer on the Pt(111) electrode at 0.7 V in 0.1 M HClO₄. The STM are collected consecutively at the same area on the Pt(111) sample in a time interval of 25 s. Scanning with a bias potential between the tip and substrate is -300 mV and a tunneling current of 1 nA. All images are 200 × 200 Å. The abrupt change seen at the upper half of panel (d) could be caused by migration of iodine adatoms on the Pt electrode.

The STM images in Figure S5 reveal that there is a brighter ($\sqrt{7} \times \sqrt{7}$)R19.1° and a dimmer ($\sqrt{3} \times \sqrt{3}$)R30° iodine adlattices in these images, they are also domains where I* adlayer do not form well-ordered structures. From the series of STM images, it can also be seen that the I* adlayer structure changes with time dynamically. This agrees well with the fact that the interaction of I* with Pt is not strong.^{2, 3}

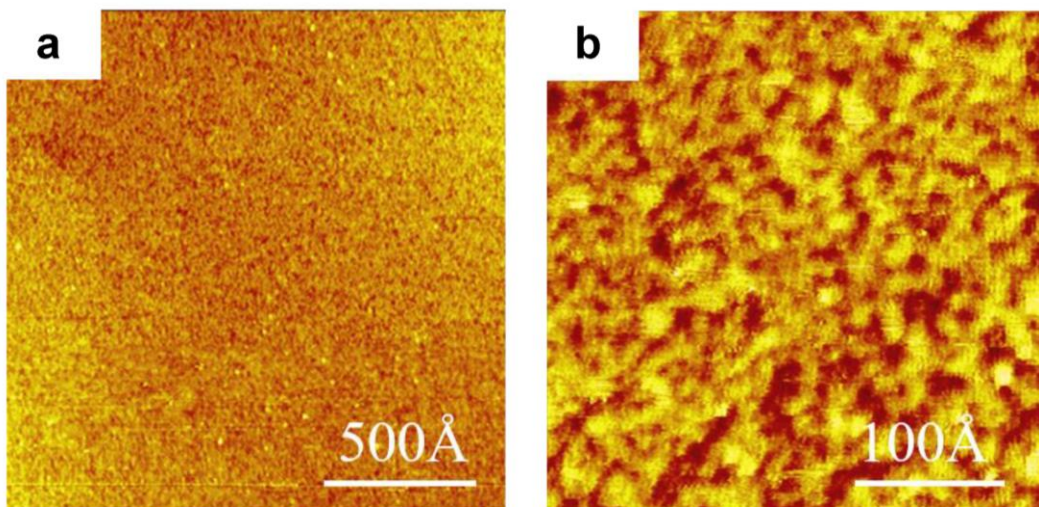


Figure S6. A large-scale of STM images showing the disordered covered iodine adlayer on the Pt(111) electrode at 0.62 V in 0.1 M HClO₄.

Shown in Figures S6a and 6b are STM images obtained at 0.62 V in 0.1 M HClO₄, which reveals that the Pt surface was universally and uniformly covered with an iodine adlayer. A finer resolution STM image shown in Figure S6b reveals that the iodine adatoms formed clusters ranging from 1 to 5 nm. It is difficult to obtain atomic resolution STM image of this iodine coated Pt(111) sample.

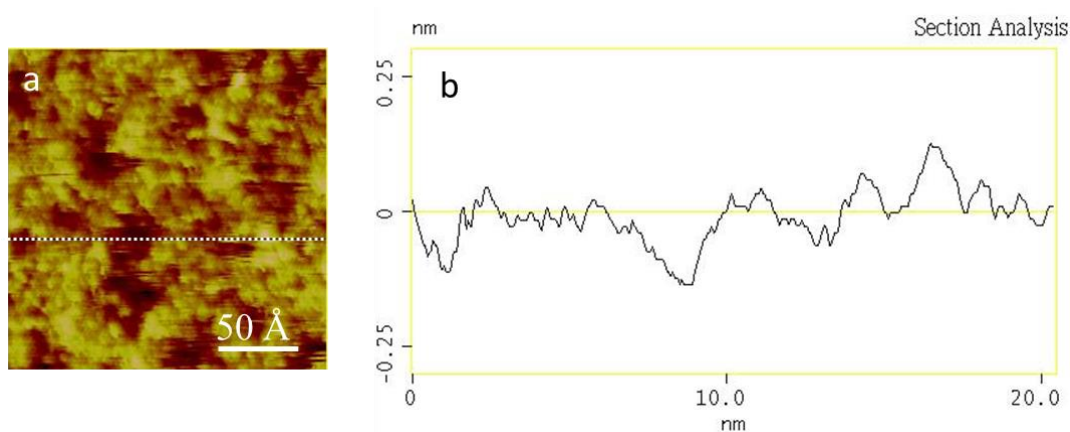


Figure S7. In situ STM image (a) and cross section profile (b). The Pt electrode was set at 0.7 V in O₂-saturated 0.1 M HClO₄ and tunneling condition is -200 mV and 1 nA. The Pt electrode surface became more corrugated with a maximal height difference of 4 Å, implying that iodine adatoms reacted with oxygen to produce uncharacterized oxide species.

The surface morphology of sample #2 exhibits significantly increased roughness upon O₂ exposure, as evidenced by the rise in corrugation height from 1.2 Å to 2.5 Å (Figure S7). This pronounced change suggests a

chemical reaction between adsorbed iodine atoms and oxygen molecules, leading to the formation of unidentified oxide species on the Pt electrode surface.

6. The structure of O₂ and H₂O adsorption on Pt surface, the charge density difference and reaction free energy were calculated by DFT.

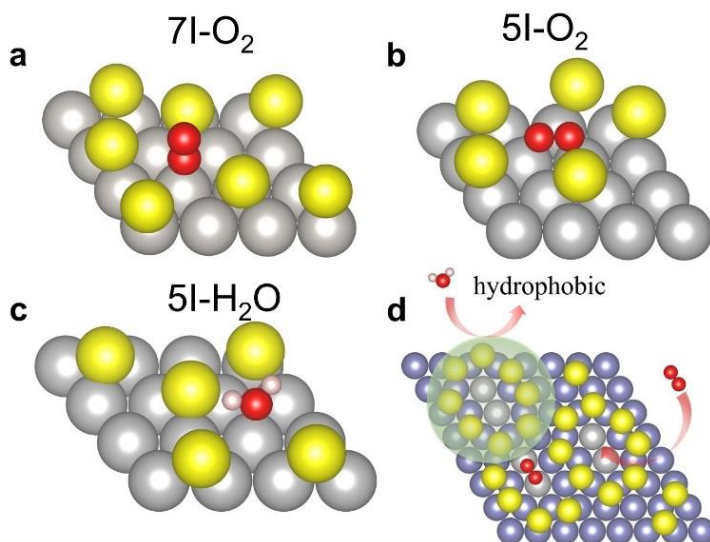


Figure S8. O₂ and H₂O adsorption structures on Pt(111)@I*, obtained by DFT calculations. (a) end-on O₂* with 7 I* on Pt(111) and $\theta_1 = 7/16 = 0.44$ ML; (b) side-on O₂*, with 5 I* on Pt(111) and $\theta_1 = 5/16 = 0.31$ ML; (c) H₂O*, with 5 I* on Pt(111); (d) model catalyst for ORR, with isolated Pt₂ units for O₂ adsorption, protected from H₂O adsorption by hydrophobic structure motifs.

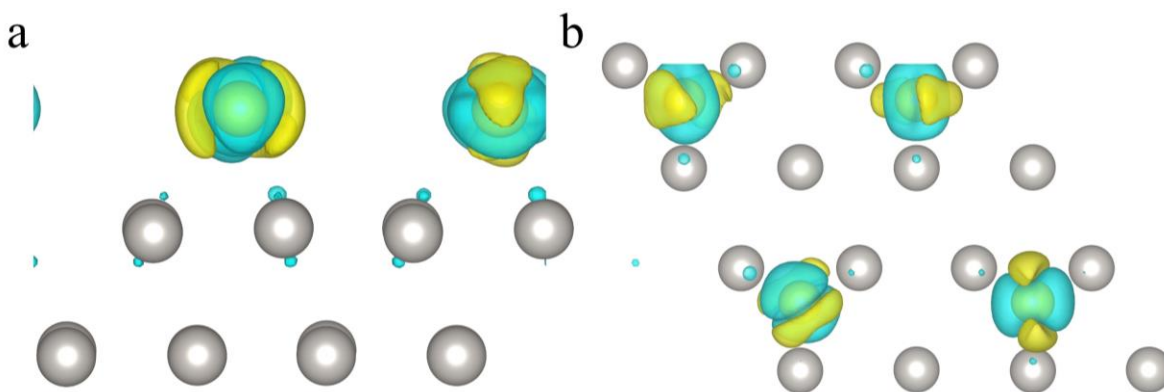


Figure S9. The charge density difference of the Pt(111) surface modified by I. (a) Top view. (b) Side view. The yellow and silver spheres represent the I atom and the Pt atom respectively. The yellow and cyan areas represent electron accumulation and consumption respectively.

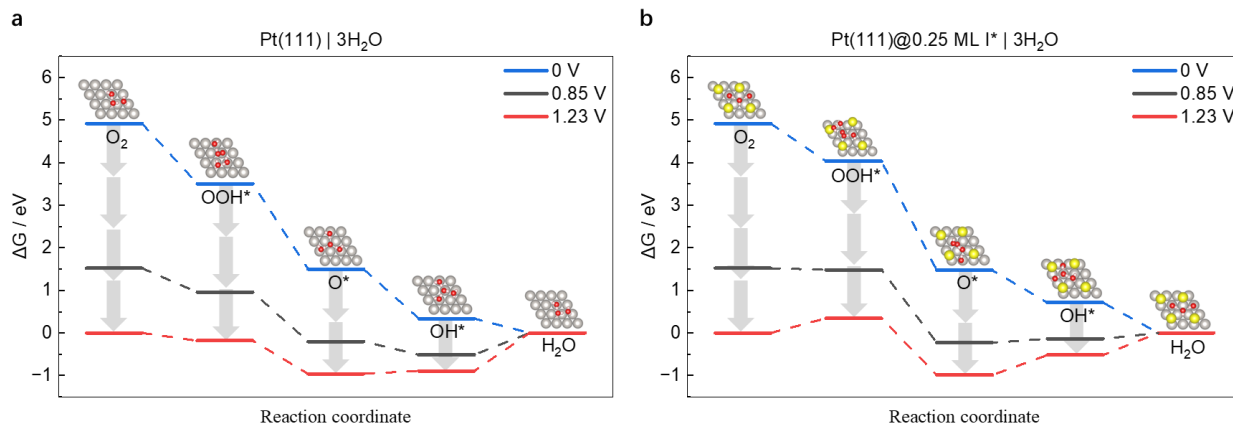


Figure S10. Free-energy diagram for oxygen reduction at three different potentials and at (a) Pt(111) | 3H₂O interface and (b) Pt(111)@0.25 ML I* | 3H₂O interface.

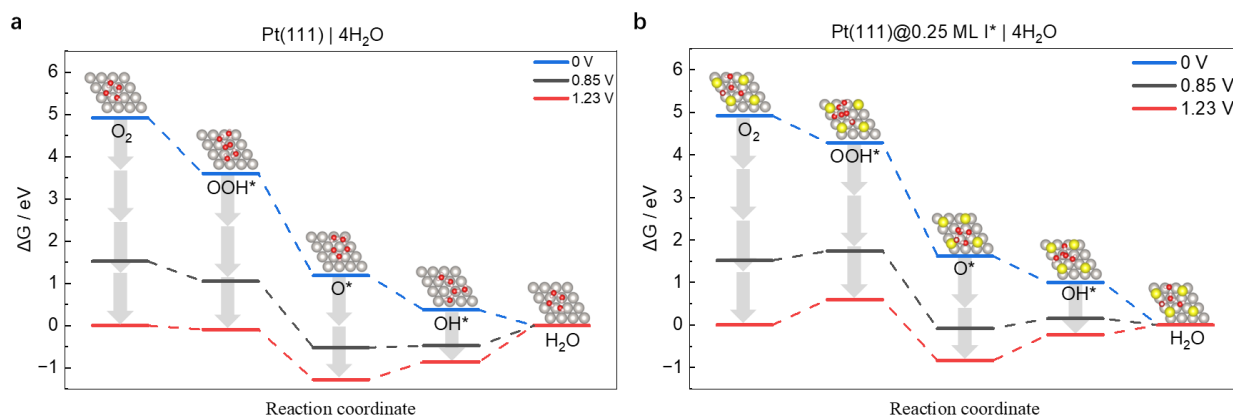


Figure S11. Free-energy diagram for oxygen reduction at three different potentials and at (a) Pt(111) | 4H₂O interface and (b) Pt(111)@0.25 ML I* | 4H₂O interface.

We calculated the reaction free energy for ORR on both clean Pt(111) and Pt(111)@I* with $\theta_I = 0.25$ ML using the Computational Hydrogen Electrode method,⁹ without applying any additional potential correction. In the adsorption models used, the adsorbed intermediates (OOH*, O*, OH* or H₂O*) are solvated by three or four explicit H₂O molecules (Figure S10 and Figure S11). Structurally, the key distinction between Pt(111) and Pt(111)@I* lies in the adsorption behavior of H₂O molecules: two H₂O molecules are adsorbed on the pristine Pt(111) surface, whereas no adsorption occurs on the I-modified Pt(111) surface. This microsolvated model captures key features of the hydrogen-bonding network and the first solvation shell at the interface, which have been shown to play an important role in tuning the reaction energetics. Therefore, the free energy changes

obtained from this model are meaningful as references for comparing the relative stability of different reaction intermediates, and they provide a rational explanation for the influence of iodine adsorption on the Pt surface in modulating the ORR.

7. The results of electrochemical in-situ ATR-SEIRAS for the Pt@I* electrode demonstrate the inhibition of I* on the H₂O*.

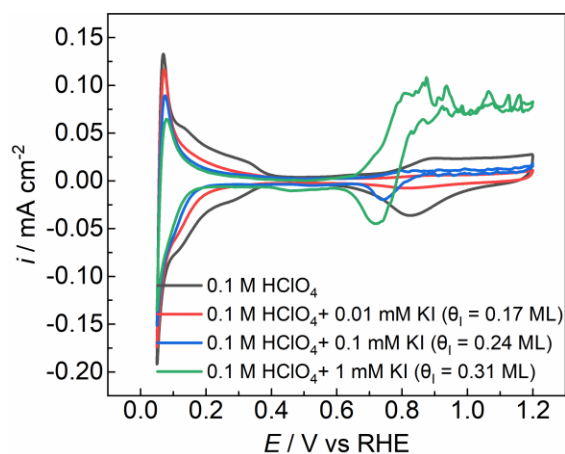


Figure S12. CVs of Pt thin film electrodes with different I* coverages in Ar-saturated 0.1 M HClO₄ for ATR-SEIRAS test.

Figure S12 displays the CVs of Pt thin film electrodes with different I* coverages in Ar-saturated 0.1 M HClO₄ by adding different concentration of KI. Similarly, the H_{UPD} and OH* regions of the Pt electrode decrease with increasing coverage. When 1 mM KI is added, an oxidation peak for I⁻ can be observed in the OH* region.

8. Evidence of positive shift in the potential of zero free charge of Pt(111)@I*/0.1 M HClO₄ interface confirms that Pt(111)@I* surface is hydrophobic

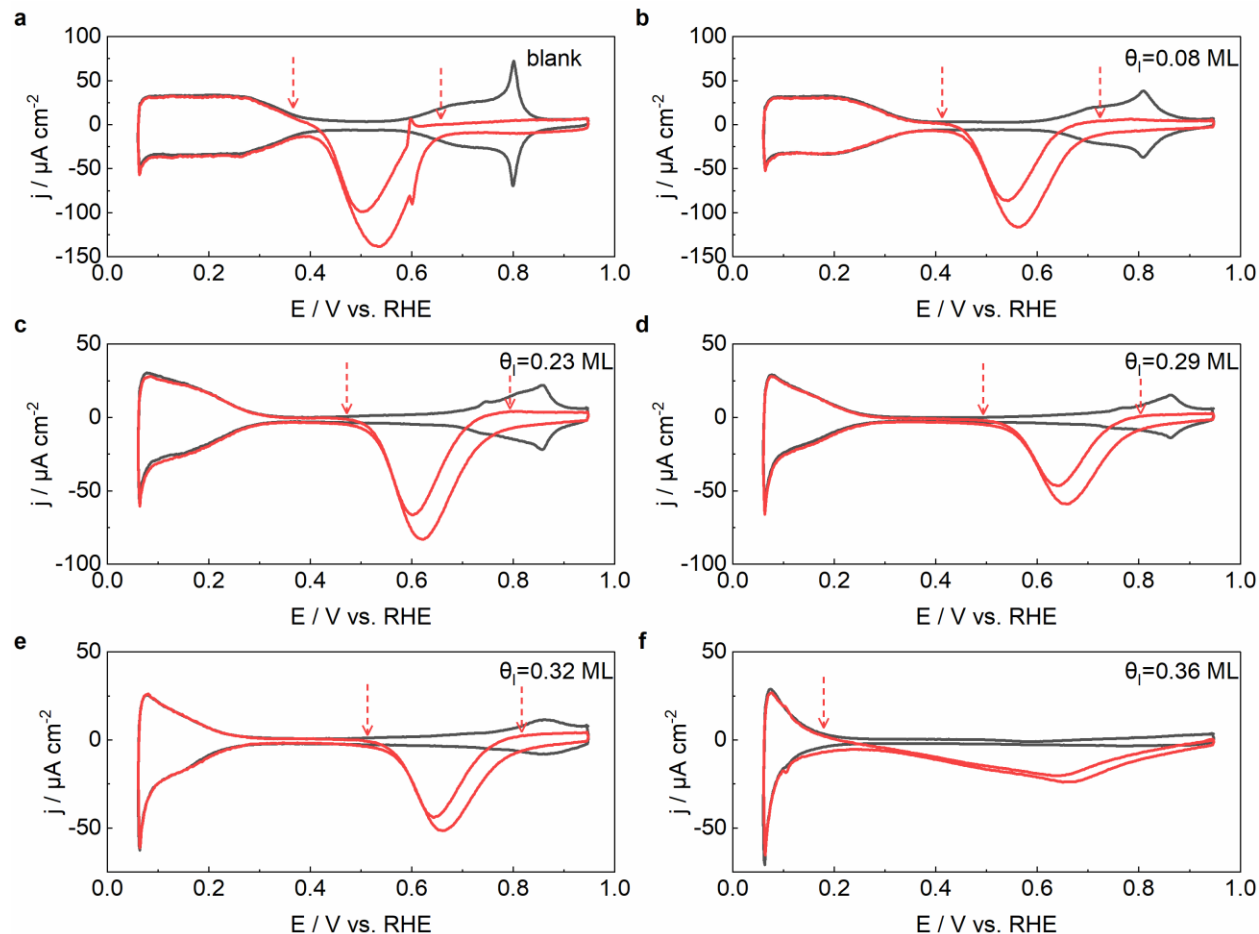


Figure S13. (a-f) Peroxodisulfate reduction (red) on Pt(111)@x ML I* electrodes in 0.1 M HClO₄ + 1 mM K₂S₂O₈. The scan rate is 50 mV/s. The blank voltammograms are also shown (black). The arrows indicate the potential of zero free charges.

The PZFC of clean Pt(111) and Pt(111)@I* with varying θ_I in HClO₄ solution, can be identified using S₂O₈²⁻ (Peroxodisulfate, PDS) reduction as the probe reaction (Figure S13). Both the higher and a lower PZFC shift positively at $\theta_I < 0.32$ ML, and shift negatively at $\theta_I > 0.32$ ML (Figure S13). On clean Pt(111), the lower PZFC is 0.362 V, in excellent agreement with previously reported value at 0.370 V.¹⁰ From $\theta_I = 0.0$, i.e. clean Pt(111) to $\theta_I = 0.32$ ML, the PZFC is shifted upward by ca. 150 mV. Considering adsorbed iodine atoms transfer a small amount of charge to Pt, this increase in PZFC must be due to a decrease in H₂O adsorption.^{11, 12} When θ_I exceeds 0.32 ML, the PZFC begins to decrease with increasing coverage. This is probably due to the weak adsorption of water renders the electronic effect of I* on Pt dominating. Due to the relatively large size of the

$\text{S}_2\text{O}_8^{2-}$ ion, the reduction current becomes very small when the iodine coverage is too high. Therefore, we only measured data within the range of 0 - 0.36 ML.

9. The ORR activity of Pt(hkl)@I* and polycrystalline Pt@I* electrodes and their kinetic current density.

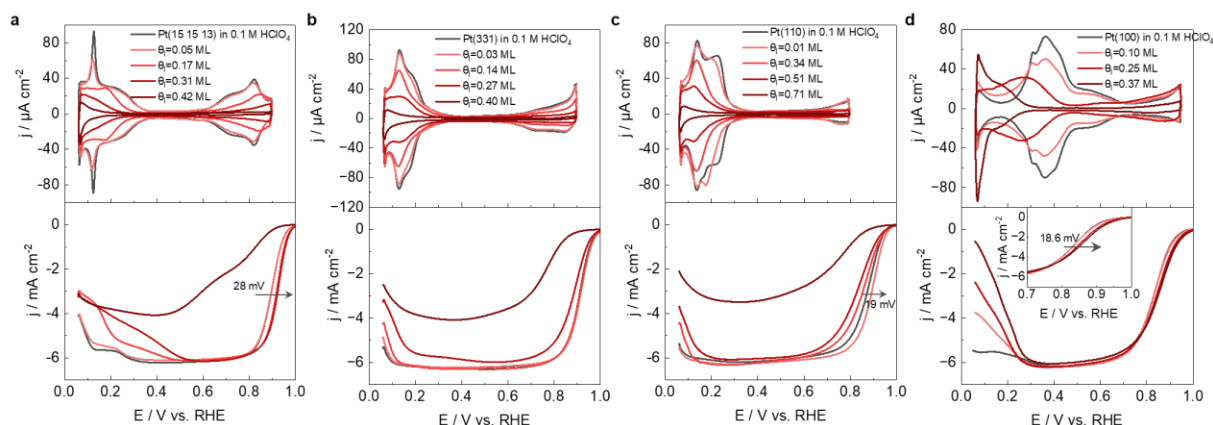


Figure S14. CVs and ORR polarization curves recorded in the positive scan in 0.1 M HClO₄ of (a) Pt(15 15 13)@ x ML I*, (b) Pt(331)@ x ML I*, (c) Pt(110)@ x ML I* and (d) Pt(100)@ x ML I* electrodes. For comparison, the base CV and the j-E curve for ORR at bare Pt(hkl) are also included in (a-d). The scan rate is 50 mV/s. For the ORR experiments, the rotation rate is 1600 rpm.

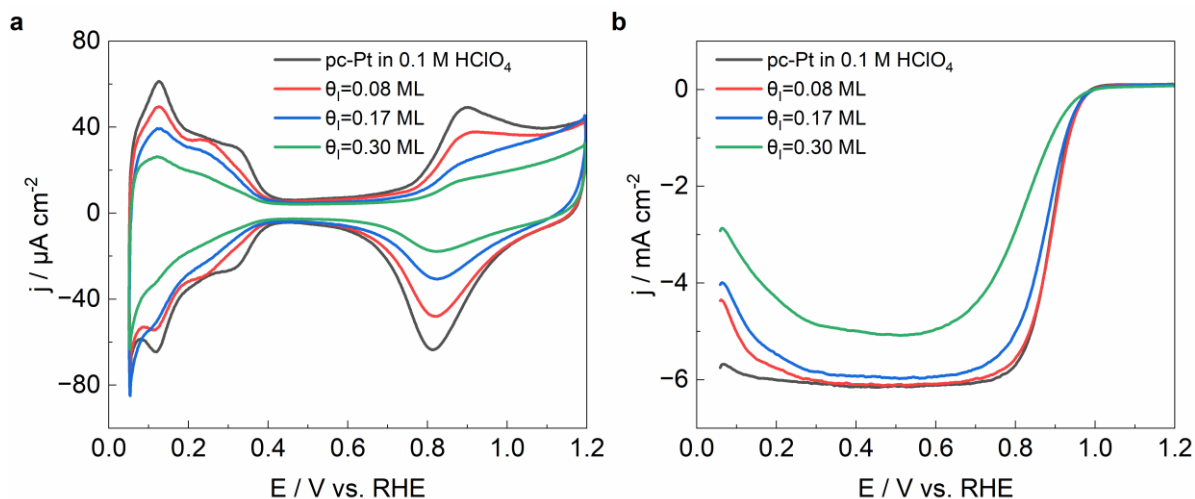


Figure S15. (a) CVs of polycrystalline Pt@I* electrodes in Ar-saturated 0.1 M HClO₄ with various coverages as indicated in the figure. (b) Positive-going j-E curves for ORR at Polycrystalline Pt@I* electrodes in O₂-saturated 0.1 M HClO₄. For comparison, the base CV and the j-E curve for ORR at bare polycrystalline Pt are also included in (a) and (b). Scan rate: 50 mV/s. For the ORR experiments, the rotation rate is 1600 rpm.

10. The Bader charge of iodine adsorbed on the Pt surface were calculated using DFT, as well as the influence of iodine on the d-band center of Pt.

Table S1. The average Bader charge of adsorbed I under different iodine coverage degrees.

The coverage of I / %	The average Bader charge of each I
6.3	0.0849
12.5	0.0783
18.8	0.0622
25.0	0.0422
31.3	0.0222
37.5	0.0269
43.8	0.0132

Table S2. The d-band center of Pt under different I coverage.

The coverage of I / %	The d-band center of the first layer of Pt/ eV	The d-band center of all Pt/ eV
0.0	-1.9570	-2.243
6.3	-2.0030	-2.234
12.5	-2.1270	-2.289
18.8	-2.1720	-2.278
25.0	-2.1720	-2.327
31.3	-2.2000	-2.294
37.5	-2.3760	-2.408
43.8	-2.2990	-2.334

References:

- (1) Göthelid, M.; von Schenck, H.; Weissenrieder, J.; et al. Adsorption Site, Core Level Shifts and Charge Transfer on the Pd(111)–I($\sqrt{3}\times\sqrt{3}$) Surface. *Surf. Sci.* **2006**, *600*, 3093.
- (2) Tkatchenko, A.; Batina, N.; Cedillo, A.; Galván, M. Charge Transfer and Adsorption Energies in the Iodine–Pt (1 1 1) Interaction. *Surf. Sci.* **2005**, *581*, 58.
- (3) Sun, C.; Wen, R.; Qin, Y.; et al. Origin of Pt Site Poisoning by Impurities for Oxygen Reduction Reaction Catalysis: Tailored Intrinsic Activity of Pt Sites. *ACS Appl. Energy Mater.* **2023**, *6*, 5700.
- (4) Lu, F.; Salaita, G. N.; Baltruschat, H.; Hubbard, A. T. Adlattice Structure and Hydrophobicity of Pt (111) in Aqueous Potassium Iodide Solutions: Influence of Ph and Electrode Potential. *J. Electroanal. Chem. Interfacial. Electrochem.* **1987**, *222*, 305.
- (5) Briega-Martos, V.; Mello, G. A.; Arán-Ais, R. M.; et al. Understandings on the Inhibition of Oxygen Reduction Reaction by Bromide Adsorption on Pt (111) Electrodes at Different Ph Values. *J. Electrochem. Soc.* **2018**, *165*, J3045.
- (6) Marković, N.; Ross Jr, P. Surface Science Studies of Model Fuel Cell Electrocatalysts. *Surf. Sci. Rep.* **2002**, *45*, 117.
- (7) Inukai, J.; Osawa, Y.; Wakisaka, M.; et al. Underpotential Deposition of Copper on Iodine-Modified Pt (111): In Situ Stm and Ex Situ Leed Studies. *J. Phys. Chem. B* **1998**, *102*, 3498.
- (8) Hubbard, A. T. Electrochemistry at Well-Characterized Surfaces. *Chem. Rev.* **1988**, *88*, 633.
- (9) Nørskov, J. K.; Rossmeisl, J.; Logadottir, A.; et al. Origin of the Overpotential for Oxygen Reduction at a Fuel-Cell Cathode. *J. Phys. Chem. B* **2004**, *108*, 17886.
- (10) Martínez-Hincapié, R.; Climent, V.; Feliu, J. M. Peroxodisulfate Reduction as a Probe to Interfacial Charge. *Electrochem. Commun.* **2018**, *88*, 43.
- (11) Li, P.; Huang, J.; Hu, Y.; Chen, S. Establishment of the Potential of Zero Charge of Metals in Aqueous Solutions: Different Faces of Water Revealed by Ab Initio Molecular Dynamics Simulations. *J. Phys. Chem. C* **2021**, *125*, 3972.
- (12) Petrii, O. Zero Charge Potentials of Platinum Metals and Electron Work Functions. *Russ. J. Electrochem* **2013**, *49*, 401.